Chemical Equilibrium Analysis of Silicon Carbide Oxidation in Oxygen and Air

Samuel Y. Chen and Iain D. Boyd

Department of Aerospace Engineering, University of Michigan, Ann Arbor, Michigan, 48109

Due to their refractory nature and oxidation resistance, Ultra-High Temperature Ceramic materials, including silicon carbide, are of interest in hypersonic aerospace applications. To analyze the thermodynamic behavior of silicon carbide during transition between passive and active oxidation states, chemical equilibrium calculations are performed. The predicted oxygen pressures for passive-to-active transition show improved agreement up to an order of magnitude with experimental transition data in the literature, compared with Wagner's model. Both oxygen and air environments are examined, and a 3% difference in transition temperature is observed. Material response analysis demonstrates that a surface temperature jump occurs during thermal oxidation of silicon carbide, corresponding to passive-to-active transition.

Nomenclature

Symbols

B'	Non-dimensional mass flux
D	Diffusion coefficient in Fick's law
δ	Diffusion length, m
C_H	Boundary layer heating coefficient
C_M	Boundary layer mass transfer coefficient
C_p	Heat capacity, J/kg-K
ε	Removal Probability
ϵ	Emissivity
F	Diffusion coefficient factor
G	Gibbs free energy, J/mol
h	Specific enthalpy, J/kg
i, k	Species
J	Species diffusion flux, $1/m^2$-s
J'	Species mass diffusion flux, kg/m^2-s
κ	Thermal conductivity, W/m-s
K_p	Equilibrium constant
Le	Lewis number
$\dot{m}$	Mass flux, kg/m^2-s
M	Molecular weight, kg/kmol
ν	Stoichiometric coefficient
P	Pressure, bar
Q	Heat flux, W/m^2
R	Universal gas constant, 8.314 J/mol-K
s, l, g	Solid, liquid, gas phase
$\dot{s}$	Surface recession rate, m/s
ρ	Density, kg/m^3
σ	Stefan-Boltzmann constant, W/m^2-K^4

T Temperature, K

X Mole fraction

u Velocity, m/s

Y Mass fraction

Subscripts

e Boundary layer edge

g Blowing gas

l Condensed phase

w Gas-surface interface

Superscripts

^{o} Standard conditions, 1 bar

Abbreviations

A-P Active-to-passive

P-A Passive-to-active

ACE Aerotherm Chemical Equilibrium

SEB Surface energy balance

SMB Surface mass balance

TGA Thermo-gravimetric apparatus

UHTC Ultra-High Temperature Ceramic

I. Introduction

Silicon carbide (SiC) is an Ultra-High Temperature Ceramic (UHTC) material that has been extensively studied for use in hypersonic leading edges and control surfaces. These are system-critical components that operate in high temperature oxidizing environments. However, SiC loses oxidation resistance around 1800 °C.[1] Under moderate heating conditions and high oxygen partial pressures, SiC forms a stable SiO_2 "passive" oxide. For practical applications, this passive mode is desired, due to its low oxygen diffusivity, preventing further oxidation of SiC. At higher temperatures and lower oxygen pressures, SiC instead oxidizes "actively," forming volatile SiO that leads to further degradation of the material.[2]

Both active-to-passive (A-P)[3,4] and passive-to-active (P-A)[5] oxidation transitions have been investigated for SiC in various oxygen mixtures and air, but there are significant differences between experimental results and existing theories. Also, combined oxidation and nitridation of SiC in air have not been sufficiently explored.[6] A "temperature jump" phenomenon[7–9] has been observed in thermal oxidation experiments with SiC composites undergoing P-A transition, characterized by an abrupt rise in surface temperature. This effect has been linked with an increase in catalycity and surface chemistry that augments the surface heating.

This work addresses surface equilibrium effects between SiC and ambient oxygen and air environments. An *open*-system mass balance is used, along with multi-component equilibrum between gaseous and condensed species. Mass transport effects in the boundary layer are approximated. Previous theoretical works have largely focused on single reaction equilibria, and neglected differences between oxygen and air environments. Wang *et al.*[10] utilized a more detailed thermodynamic approach, but only to identify key species. Poerschke *et al.*[11] and Dawi *et al.*[12] performed a thermodynamic analysis to determine transition condi-

tions, but Wang, Poerschke, and Dawi considered a *closed* system, and did not account for boundary layer diffusion.

In this paper, experiments and theories in the literature that describe both A-P and P-A transitions are first briefly reviewed. Detailed thermodynamic equilbrium calculations are performed to understand the significance of diffusive and thermodynamic effects in oxidation of SiC. P-A transitions predicted with this approach are compared to experimental data in the literature for both oxygen and air. Finally, implications for the temperature jump phenomenon are considered, and an explanation for the temperature jump is proposed based on the thermodynamic calculations.

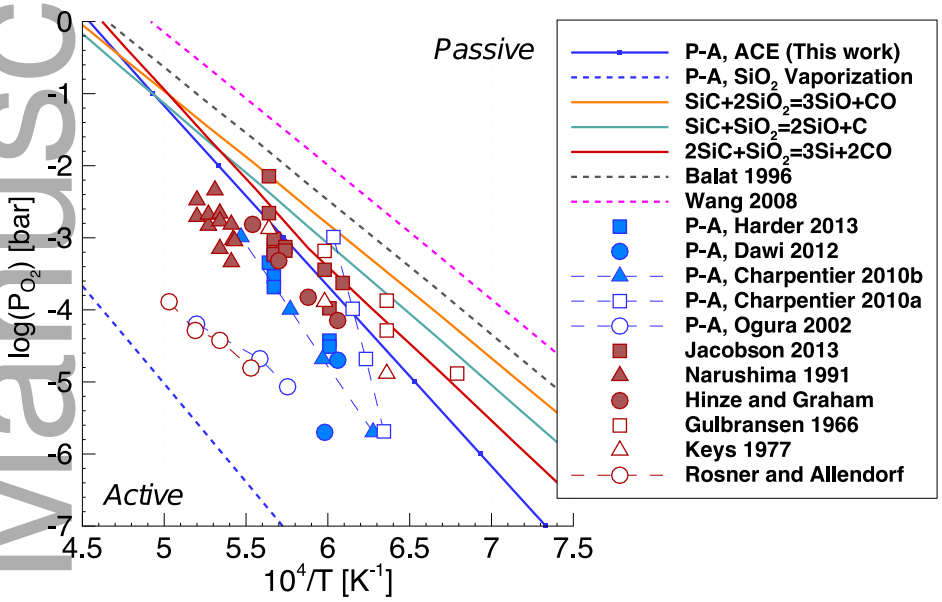

Figure 1: Summary of experimental (symbols) and theoretical (lines) transition conditions for SiC-O_2. Data for air is excluded. Both active-to-passive and passive-to-active transitions are shown, and correspond to active-to-passive unless otherwise indicated.

II. Experimental Data

The oxygen pressures and temperatures where both A-P and P-A oxidation transitions occur are compiled from various experiments in the literature. Figure 1 summarizes the transition data for the SiC-O_2 system from several experiments.[2,3,5,12–19] Symbols denote experimental data, and lines denote theoretical/computed results, discussed in the following sections.

Experimental conditions span a range of total pressures from 1.0×10^{-4} to 1.0 bar. Inert gases such as argon and helium are used to dilute O_2 mixtures and achieve higher total pressures.[20] It has been shown in theory and literature that the transition points are relatively independent of the total pressure and addition of inert diluents. The gas compositions used in these experiments include pure O_2, Ar-O_2, and He-O_2,

but not air (N_2-O_2). Nitrogen is not strictly inert with SiC, and has a coupling effect with oxygen due to nitridation,[6] as discussed in the air results section.

The scatter in the data can be accounted for by facility effects, SiC polytype and microstructure, composition (including impurities), and transition criterion.[14] Most transition data for the SiC-O_2 system appear to be clustered in Fig. 1, and represent oxidation experiments performed in a diffusion-limited regime. However the results of Dawi,[12] Ogura,[15] and Rosner[18] were obtained from experiments performed at very low oxygen pressures, and represent a reaction-limited regime. The experimentally observed dependence of oxidation transitions on bulk transport and flowrate may be indicative of deviation from diffusion-limited equilibrium conditions, as demonstrated by Narushima.[19]

III. Theoretical Models

Theories describing the active-to-passive[2,4,10,16] or passive-to-active[5] transitions are based on chemical/thermodynamic equilibrium of one or more reactions. For each reaction i, the standard free energy ΔG^o can be computed using species thermochemical data,[21] and minimization of the system's free energy results in Eq. (1).[22]

$$K_{p,i} = \exp\left(\frac{-\Delta G^o}{RT}\right) \tag{1}$$

The equilibrium constant, K_p, is used to determine the equilibrium vapor pressures for homogeneous or heterogeneous gas reactions, which are then combined with a boundary layer diffusion model based on either Wagner's[23] (illustrated in Fig. 2) or Turkdogan's[24] theory. These models have largely focused on the interaction of SiC with O_2, although a limited number of studies address the effects of N_2.[7,25] Both A-P and P-A transitions are discussed in this section, and the results are shown in Fig. 1 as lines.

However, the wide range of the data suggests that it may not be possible to reach equilibrium at the SiC interface. Wang *et al.*[10] suggest that the partial pressures of SiO, CO, and O_2 are very far out of equilibrium with respect to the equilibrium vapor pressures. Chemical kinetics and species diffusion can have competing effects in the boundary layer, and present a barrier to reaching equilibrium. Additionally, equilibrium analysis based on a limited set of reactions may be insufficient, which will be addressed in the chemical equilibrium approach.

III.A. Active-to-Passive Transitions

Active oxidation of SiC proceeds according to Eq. (2):

$$\mathrm{SiC}(s) + \mathrm{O_2}(g) \rightarrow \mathrm{SiO}(g) + \mathrm{CO}(g) \tag{2}$$

Transition models for SiC[2,4,10,16] based on Wagner's theory of pure silicon oxidation[23] represent a diffusion-limited regime. Fick's law in Eq. (3) describes the diffusion flux J_i of species i towards the surface through the boundary layer:

$$J_i = D_i \frac{P_{e,i} - P_{w,i}}{\delta_i} \frac{1}{RT} \tag{3}$$

Figure 2 illustrates that there will be a flux of O_2 towards the surface, and a flux of oxidation products away from the surface.

According to Wagner' theory, the equilibrium vapor pressures of SiO(g) and CO(g) determine the maximum flux of O_2(g) consumed at the SiC surface for a given temperature, and correspond to the A-P transition point. The oxygen pressure in the ambient, P_{e,O_2}, that corresponds to transition is determined by approximating the O_2(g) gradient in the boundary layer with Fick's law.[2] Condensation of SiO_2(s) either from the ambient or directly from reactions with SiC leads to the passive oxidation state, and occurs when oxygen pressures exceed the A-P ambient oxygen pressure.[25]

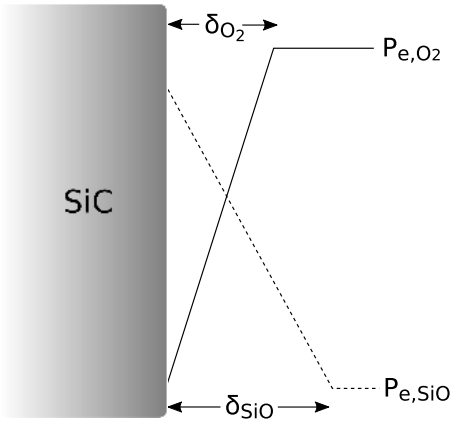

Figure 2: Wagner model for active SiC oxidation.

Reactions describing the critical SiO(g) and CO(g) vapor pressures for SiO_2(s) condensation have been proposed by various researchers.[4,10] Gulbransen *et al.* proposed Eqs. (4) - (6),[16] and Fig. 1 shows that the A-P transitions predicted with Wagner's model are clearly sensitive to the choice of reaction.

$$\mathrm{SiC}(s) + 2\mathrm{SiO_2}(s) \rightarrow 3\mathrm{SiO}(g) + \mathrm{CO}(g) \tag{4}$$

$$\mathrm{SiC}(s) + \mathrm{SiO_2}(s) \rightarrow 2\mathrm{SiO}(g) + \mathrm{C}(s) \tag{5}$$

$$2\mathrm{SiC}(s) + \mathrm{SiO_2}(s) \rightarrow 3\mathrm{Si}(l) + 2\mathrm{CO}(g) \tag{6}$$

The transition line predicted with Eq. (6) provides the best agreement with experimental data, although condensed silicon has not been observed in experiments.[4,3] These reactions describe equilibrium between SiO_2(s) and SiC(s), and indicate that SiO_2(s) is thermodynamically stable only when there is sufficient

SiO(g) or CO(g) pressure at the surface for SiC(s)-SiO_2(s) equilibria.

III.B. Passive-to-Active Transitions

In the passive oxidation regime, the loss of the protective SiO_2(s) oxide characterizes transition to active oxidation. Contrary to pure silicon, Harder and Jacobson[5,20] showed that A-P and P-A transitions for SiC are similar, and propose that a weak hysteresis exists. The experimental transition data in Fig. 1 confirm the similarity of both transitions, but hysteresis is rather inconclusive. In fact, in the literature, predictions for A-P transition[4] have been applied to data from P-A experiments, and compare well.[26,9]

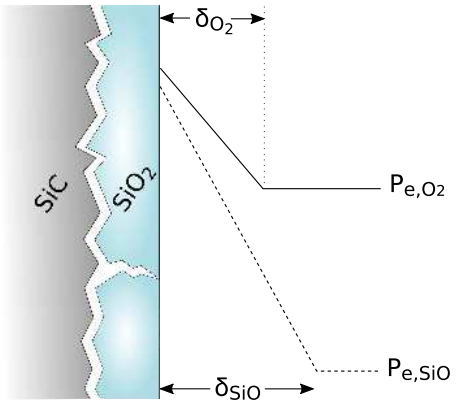

Figure 3: Wagner model applied to passive SiO_2 vaporization.

Dissociative vaporization of SiO_2(s) at the gas interface via Eq. (7) is a potential mechanism for P-A transition:

$$SiO_2(s) \rightarrow SiO(g) + \frac{1}{2}O_2(g) \tag{7}$$

This mechanism is evaluated with a modified Wagner model illustrated in Fig. 3, where both O_2(g) and SiO(g) diffuse away from the surface. The transition line calculated for SiO_2(s) vaporization is plotted in Fig. 1, and occurs at oxygen pressures that are three orders of magnitude lower than those observed in experiments, as verified by Harder *et al.*[5] Thus, SiO_2(s) vaporization is not the primary mechanism for P-A transition.

Models based on Turkdogan's theory of vaporization[24] agree better with observed data, but are difficult to generalize without detailed information about the experimental conditions and facilities, such as the flowrates and velocities outside the boundary layer. However, Harder *et al.* demonstrated that transition oxygen pressures predicted with this approach still differ from experimental P-A data by one to two orders of magnitude.[5]

Figure 3 illustrates another important mechanism for SiO_2(s) consumption: substrate reactions between SiC(s) and SiO_2(s). This mechanism is described via Eqs. (4) - (6), where both SiC(s) and SiO_2(s) are consumed at the SiC(s)-SiO_2(s) interface, and can lead to pressure build-up of SiO(g) and CO(g). This build-up can lead to mechanical rupturing of the thinning SiO_2(s) layer, exposing bare SiC(s) to O_2(g) and causing transition to active oxidation before the thermodynamic equilibrium condition.[2,5] Equilibrium between SiC (substrate) and condensed species cannot be adequately described by a Wagner- or Turkdogan-

based diffusion model.

A modified Deal-Grove model[27] has been shown to accurately describe the oxidation of SiC crystals under moderate, passive oxidation conditions, including the growth rate of the SiO_2(s) layer by accounting for oxidant diffusion through the SiO_2(s) into the SiC(s)-SiO_2(s) interface. However, at active oxidation conditions SiO_2(s) is not thermodynamically stable, and growth of the oxide layer will not occur. This limits the usefulness of the Deal-Grove model in analyzing P-A transition.

IV. Chemical Equilibrium Model

IV.A. Principles and Governing Equations

An open system mass balance is used to evaluate mass fluxes at the surface, illustrated in Fig. 4. This approach relies upon assumptions of constant Prandtl and Lewis numbers, allowing the boundary layer mass and energy conservation equations to be written in terms of dimensionless mass and heat transfer coefficients, C_M and C_H:

$$Q_w = \rho_e u_e C_H (h_e - h_w) \tag{8}$$

$$Le = \frac{C_H}{C_M} \tag{9}$$

Here Q_w is the surface heat flux. Using similarity arguments, the flux of a species (e.g. SiO, O_2) can be written as:

$$J_i' = \rho_e u_e C_M (Y_e - Y_w) \tag{10}$$

J_i' is the mass flux of a species i to/from the surface, Y_e is the mass fraction of a species at the boundary layer edge, and $\rho_e u_e C_M$ is the bulk mass flux from the ambient to the surface. To account for various boundary layer compositions, a bifurcation approximation to the binary diffusion coefficients for species i into j is evaluated according to the correlation of Bartlett *et al.* in Eq. (11):[28]

$$D_{ij} = \frac{D_{\text{ref}}}{F_i F_j}, \quad F_i = \left(\frac{M_i}{26.0}\right)^{0.461} \tag{11}$$

D_{ref} is the self-diffusion coefficient of O_2, used as a reference value for this correlation, and F_i is the "diffusion factor" for species i. This correlation is shown to be accurate to within 15% for species differing up to an order of magnitude in molecular weight.[28]

Mass conservation at the gas-surface interface dictates that the blowing mass flux *into* the gas-surface interface, $\dot{m}_g$, must equal the net mass flux *away* from the surface, $\dot{m}_w$. This quantity is non-dimensionalized

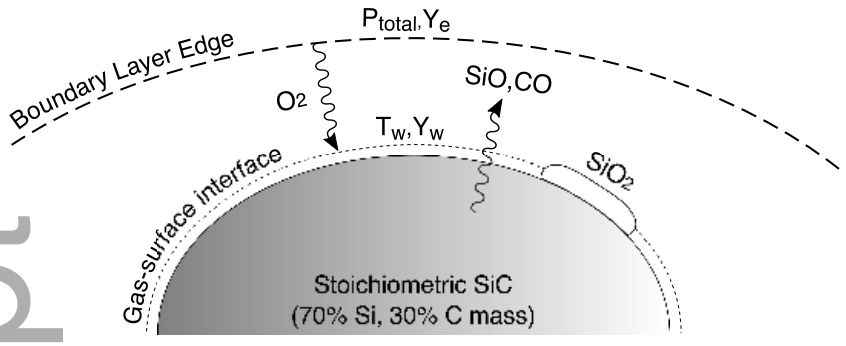

Figure 4: Open system mass balance in ACE. Three regions are present: the boundary layer edge, the gas-surface interface, and the bulk material. O_2 species represent the flux $\rho_e u_e C_M$ from the ambient to the surface, and SiO/CO represent the flux of oxidation products away from the surface $\dot{m}_w$. Flow outside the boundary layer is $\rho_e u_e$.

into the parameter B' as follows:

$$\underbrace{B'}_{\text{non-dimensional}} = \overbrace{\frac{\dot{m}_g}{\rho_e u_e C_M}}^{\text{into gas-surface interface}} = \overbrace{\frac{\dot{m}_w}{\rho_e u_e C_M}}^{\text{away from surface}} \tag{12}$$

The main assumption used in these computations is equilibrium between gaseous species and the surface, including any condensed phase species. Overall conservation of mass and elements is maintained by balancing boundary layer diffusion fluxes, convective fluxes, and ablative/blowing fluxes from the wall. For a simplified case with *equal* diffusion coefficients and no condensed phase material removal, mass balance at the gas-surface interface determines the mass fraction of a species, Y_w:

$$\rho_e u_e C_M (Y_w - Y_e) + \dot{m}_w Y_w = \dot{m}_g Y_g \tag{13}$$

$$Y_w = \frac{B' Y_g + Y_e}{1 + B'} \tag{14}$$

Thus, the B' value parameterizes the composition at the gas-surface interface by increasing the contribution of species and elements from the surface. An analogous expression can be derived for *unequal* diffusion coefficients, and accounting for condensed phase species, which is used in this work.[29]

The Aerotherm Chemical Equilibrium (ACE) program[29] is utilized for this work. ACE is a combined mass transport and thermodynamic equilibrium code, and solves the simplified multicomponent boundary layer diffusion equations described here. Thermodynamic equilibrium of a system is both reaction- and path-independent. To compute the species concentrations for a system in thermodynamic equilibrium, the specific reactions involved need not be considered. The formation of each species i can be written as the sum of constitutive species k. For SiC-O_2, constitutive species include O_2(g), SiO(g), and CO(g). All other species are formed by combinations of these species. This process is generalized in Eq. (17), and is performed

automatically in ACE.

$$\underline{\text{Example:}}\quad \underbrace{\mathrm{SiO}(g)+\mathrm{CO}(g)}_{\text{Constitutive}} = \underbrace{\mathrm{Si}(g)+\mathrm{CO_2}(g)}_{\text{Gaseous}} \tag{15}$$

$$\underline{\text{Example:}}\quad \underbrace{\mathrm{SiO}(g)+\mathrm{CO}(g)}_{\text{Constitutive}} = \underbrace{\mathrm{SiC}(s)}_{\text{Condensed}} + \underbrace{\mathrm{O_2}(g)}_{\text{Constitutive}} \tag{16}$$

$$\sum_k \nu_{k\to i} k \longrightarrow i \tag{17}$$

$\nu_{k\to i}$ is the stoichiometric coefficient to form species i from k, and can be positive (reactant) or negative (product).

Next, the equilibrium constant for the formation of each species from Eq. (17) is computed from NIST-JANAF thermochemical data[21] according to Eq. (1). This determines the partial pressure P_i for gaseous species i:

$$\underline{\text{From (15):}}\quad K_{p,\mathrm{Si}} = K_{p,\mathrm{CO_2}} = \frac{P_{\mathrm{Si}} P_{\mathrm{CO_2}}}{P_{\mathrm{SiO}} P_{\mathrm{CO}}} \tag{18}$$

$$K_{p,i}(T) = P_i \left(\prod_k P_k^{\nu_{k\to i}} \right)^{-1} \tag{19}$$

$$\ln K_{p,i}(T) = \ln P_i - \sum_k \nu_{k\to i} \ln P_k \tag{20}$$

For each species in consideration, the equilibrium constant $K_p(T)$ is only a function of temperature. Temperature is iterated until the equilibrium condition in Eq. (20) and conservation of elements are satisfied, and partial pressures sum to the total pressure:

$$\sum_i P_i = P_{total} \tag{21}$$

Finally, as gaseous species are in equilibrium with the surface, condensed species i are determined by Eq. (23).

$$\underline{\text{From (16):}}\quad K_{p,\mathrm{SiC}} = \frac{P_{\mathrm{O_2}}}{P_{\mathrm{SiO}} P_{\mathrm{CO}}} \tag{22}$$

$$\ln K_{p,i}(T) \geq -\sum_k \nu_{k\to i} \ln P_k \quad \begin{cases} \text{if} \quad = \quad \text{then } i \text{ is present as a condensed species;} \\ \text{if} \quad > \quad \text{then } i \text{ is not present in equilibrium.} \end{cases} \tag{23}$$

Note that Eq. (23) applies for the bulk material and any condensed species. The pressure and composition of the boundary layer edge is specified according to the ambient environment (e.g. pure O_2 or air), and assumed to be constant/frozen. In practice, only the total pressure and the elemental mass fractions at the

boundary layer edge and in the bulk material are specified, and the system is solved for various values of B'. The mixture thermodynamic properties of the gas at the wall is then computed. Additional details can be found in the ACE User Manual.[29]

IV.B. Transition Criterion

Each B' value corresponds to a unique solution of temperature and pressure (but not vice-versa, since multiple phases may exist at the same the temperature). Furthermore, B' values are used to delineate active and passive oxidation states. The transition criterion used in this work is the state where *SiO_2 begins/ceases to be a stable condensed phase.*

For SiC oxidation, the thermodynamics of both A-P and P-A systems are similar, but the mechanism of each transition is different. This criteria neglects the respective mechanisms that lead to hysteresis in A-P vs. P-A transitions, and simply determines the thermodynamic state required for stability of SiO_2 and hence transition. For example, the consumption of the SiO_2 below the silica layer is the driving factor for P-A transitions.[5] However, for the P-A transition, the equilibrium approach cannot account for rupture of the silica layer (bubbling). Ogura and Morimoto showed that there exists an intermediate "passive-to-bubble" transition[15] that is not accounted for in this approach, since bubbling is the result of substrate reactions.

For Ar-O_2 environments, surface oxidation is driven by flux of oxygen from the ambient to the surface. B' represents the flux of oxidation products away from the surface, normalized by the incident flux of all species, including oxygen and inert argon. For dilute mixtures of oxygen, the partial pressure of oxygen in the ambient determines the absolute flux of oxygen to the surface. Thus, the critical B' value at which transition occurs is proportional to the ratio of oxygen pressure to total pressure:

$$B'_{\text{crit}} \propto \frac{P_{\text{O}_2}}{P_{\text{total}}} \tag{24}$$

B' values below this correspond to the passive oxidation state, while values above correspond to the active oxidation state.

V. Results

As mentioned by Rosner and Allendorf, a thermodynamic approach alone is insufficient to determine the transition accurately.[18] Models based on one or two specific reactions also underpredict transition temperature and overpredict P_{O_2}. Thus, effects of boundary layer diffusion, condensed species, and reaction-independence on gas-surface equilibrium are included with this approach. However, kinetic and nonequilibrium effects are still omitted.

V.A. Pure O_2 and Ar-O_2

The four elements considered in these cases are Si, C, O, and Ar. The bulk material consists of Si and C in a stoichiometric ratio, and the mass fractions of O and Ar at the boundary layer edge are adjusted to achieve the desired P_{O_2} at a given total pressure. SiO_2, Si(l), and C(s) are the condensed phase species included in the analysis.

Transition oxygen pressures from 1.0 from 1.0×10^{-8} bar, and total pressures from 1.0 to 1.0×10^{-3} bar fall on the same "ACE" line shown in Fig. 1. There are negligible differences observed between O_2 and Ar-O_2 environments. This implies that P-A transition for the SiC-O_2 system is relatively independent of total pressure and presence of inert diluents. There is nearly two order of magnitude scatter in the experimental data in Fig. 1. Compared to existing models in the literature, the ACE transition line improves agreement with experimental results, and agrees with most data within an order of magnitude oxygen pressure.

The isobaric B' plots in Figs. 5 and 6 are representative of solutions for SiC-Ar/O_2 systems, and show the relationship between temperature, mixture thermodynamic properties, surface mass flux, and species concentrations. The P-A transition point occurs at $B'_{crit} = 2.1 \times 10^{-1}$ in Figs. 5 and 6, and separates the passive regime (with SiO_2 surface) from the active (SiC surface). Left and right sides of the plots correspond to passive and active oxidation states, respectively.

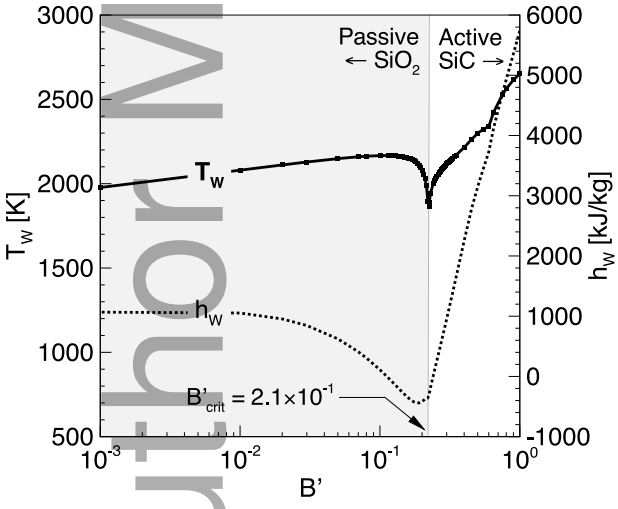

Figure 5: B' plot for the SiC-Ar/O_2 system, P_{total} = 1.00×10^{-3} bar, P_{O_2} = 2.12×10^{-4} bar. The transition point separates passive (SiO_2) and active (SiC) regimes.

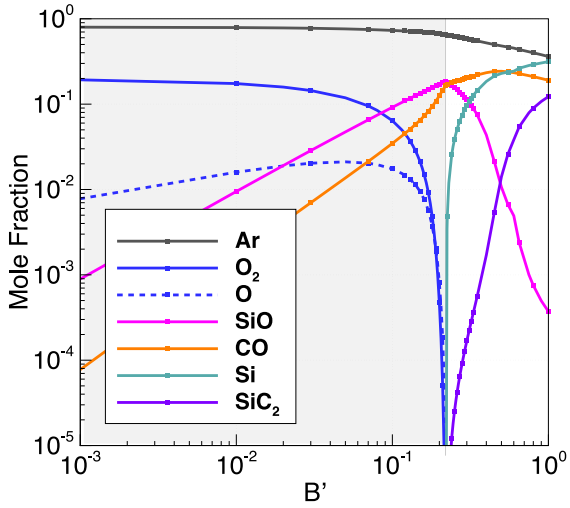

Figure 6: Gas-phase equilibrium species composition for the SiC-Ar/O_2 system, P_{total} = 1.00×10^{-3} bar, P_{O_2} = 2.12×10^{-4} bar. Passive oxidation is denoted by the shaded region.

In Fig. 6, the concentrations of both molecular and atomic oxygen indicate that they are inactive at the surface in the passive oxidation regime, but are completely consumed past the transition point, which is characteristic of active oxidation. During passive oxidation, higher surface mass loss rates (B') lead to increased partial pressures of SiO(g) and CO(g) until the P-A transition point is reached. The relative

concentration of argon *decreases* at the surface during active oxidation according to Eq. (14). This indicates outgassing from the surface consistent with higher surface mass loss rates during active oxidation. Si(g) and SiC_2(g) are present in the active region, but do not contribute to P-A transition.

V.A.1. Predominant Condensed Phase

In the chemical equilibrium analysis, the condensed surface species are determined with Eq. (23), and depend on the local values of B', T_w and P_{O_2}. The predominant surface phase as a function of B' is shown in Fig. 7(a). For passive oxidation, the surface is predominantly SiO_2(s), and is stable at low B' values. Physically, SiO_2 forms a barrier to oxygen diffusion onto the surface, and thus oxygen is unable to react with SiC. This same effect is modeled at small B' values, since the mass fraction of Si-C at the gas-surface interface is proportional to B', according to Eq. (14). P-A transition occurs at the boundary of the SiO_2(s) stability region.

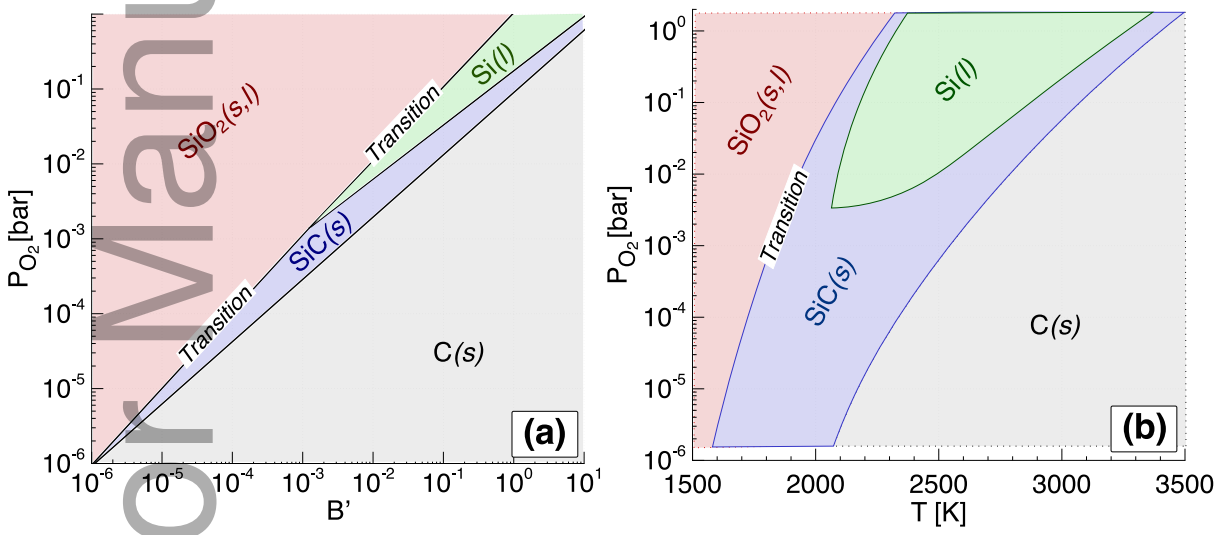

Figure 7: Predominant surface phase maps for the SiC-Ar/O_2 system at constant total pressure of 1.0 bar, (a) as a function of B', and (b) as a function temperature. Passive-to-active oxidation transitions occur at the boundary of the SiO_2(s) stability region.

Since each B' value corresponds to a temperature in Fig. 5, condensed species are mapped as a function of temperature in Fig. 7(b). However, multiple B' values may correspond to the *same* equilibrium temperature, so the mapping of temperature to B' is not unique as seen in Fig. 5, and are characterized by different surface compositions. It follows that the most thermodynamically stable phase at each temperature can be determined from free energy minimization, and these are mapped in Fig. 7(b). Figure 7(b) is not strictly a predominance diagram, since temperature is varied.

Surface equilibria with both SiC and graphite are consistent with theoretical[25] and experimental[30] descriptions of active SiC oxidation. Sooting is known to occur for SiC at temperatures higher than the

transition temperature (above 2200 K).[18] Above 2000 K and 10^{-3} bar oxygen pressure, condensed silicon is predicted to be stable, and the stability region grows with increased oxygen pressure. Condensed silicon can be explained with Eq. (6), but has not been observed in any experiments. However, only a limited number of experiments involve temperatures above 2000 K at this pressure regime.[26,9] During active oxidation, a thin layer of condensed silicon is easily volatilized into gaseous Si, and may only be present in-situ.

V.B. Air

Limited comparisons have been made between pure O_2 and N_2-O_2 conditions in the literature. Experiments investigating SiC oxidation in air have typically neglected the effects of N_2. Rosner and Allendorf studied SiC under mixtures of atomic nitrogen and oxygen,[6] dissociated at reduced temperatures using a microwave discharge facility, and observed some coupling effects between the N and O atoms.

To evaluate oxidation in air, four elements are considered in the analysis: Si, C, N, and O. Again, the bulk material consists of Si and C in a stoichiometric ratio. The N and O mass fractions in air (76.5% N, 23.5% O) are imposed at the boundary layer edge. In addition to the species considered in the Ar/O_2 case, Heuer and Lou suggest that gaseous SiN(g), Si_2N(g), Si_3N_4(s), and Si_2N_2O(s) are relevant, and are thus included in the analysis.[25] Note that NIST-JANAF tables do not contain Si_2N_2O(s), and thermodynamic data from Fegley was used for this specie.[31]

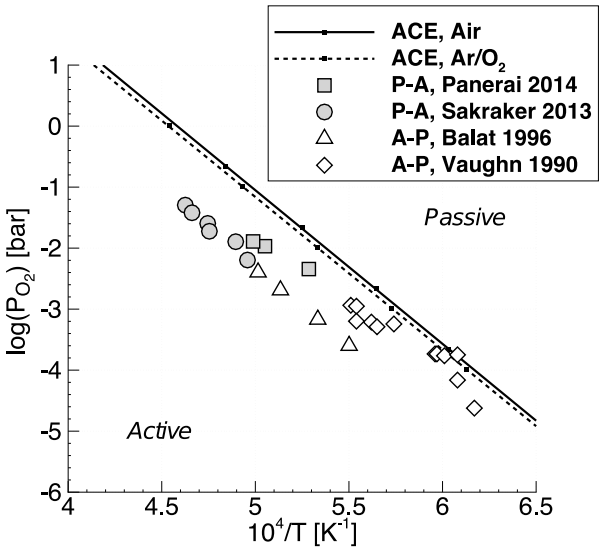

Figure 8: Oxidation transitions for the SiC-air system, both passive-to-active and active-to-passive. The Ar/O_2 transition is also shown for comparison. Symbols denote experimental data.

For the SiC-air system, Fig. 8 shows the P-A oxidation line computed with the chemical equilibrium approach. The P-A transition for the SiC-Ar/O_2 system is also plotted for comparison, and is nearly identical to the air results, occurring at slightly lower temperatures/higher oxygen pressures. Experimental data for SiC-air from Panerai[9] and Vaughn[32] compare very well with the both lines, although transition oxygen

pressures from Balat[4] and Sakraker[26] are an order of magnitude lower. The measurements of Panerai and Sakraker were taken at high flowrate conditions, and may deviate from a diffusion-limited regime.

For the same $P_{O_2} = 2.12 \times 10^{-4}$ bar, Fig. 9 shows the isobaric plots of T_w and h_w for both air and Ar/O_2, and there are slight differences in thermodynamic behavior between the two systems when argon is replaced with nitrogen. Notably, the transition temperature occurs ~3% lower for SiC-air, and at higher mass loss rates ($B'_{crit} = 0.30$ vs. 0.21). Wall enthalpy differences in the passive regime can be attributed to the higher specific heat of N_2 over Ar.

Gaseous species over the same range of conditions are described in Fig. 10. For equilibrium wall temperatures between 1500 K and 2500 K, N_2 is negligibly dissociated, as the mole fraction of atomic nitrogen is on the order of 10^{-7}. Nitrogen appears to be relatively inert with both SiO_2 and SiC in approximately equi-molar oxygen mixtures. Condensed surface species follow the SiC-Ar/O_2 case, and neither Si_3N_4(s) nor Si_2N_2O(s) are observed below air pressures of 1.0 bar. More importantly, nitrogen-bearing species do not appear in the passive region, other than N_2/N. Altogether, this suggests that passive-active transition is similar for both SiC-air and SiC-Ar/O_2 systems, and dominated by oxidation.

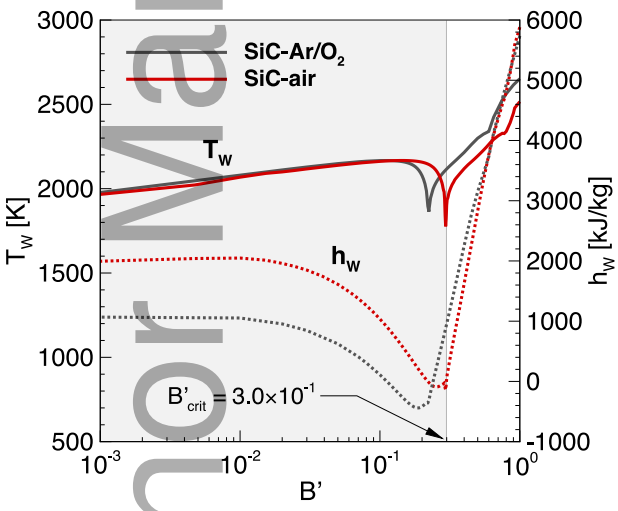

Figure 9: B' plot for SiC-air system, $P_{total} = 1.00 \times 10^{-3}$ bar, $P_{O_2} = 2.12 \times 10^{-4}$ bar. The SiC-Ar/O_2 case at equivalent P_{O_2} from Fig. 5 is shown for comparison. Shaded region corresponds to passive oxidation.

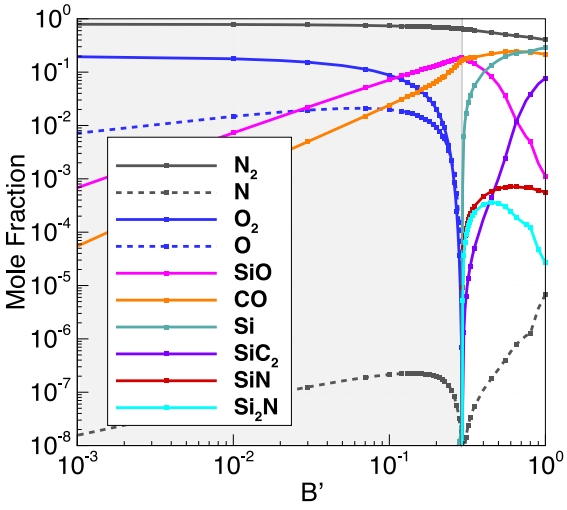

Figure 10: Gas-phase equilibrium species composition for the SiC-air system, $P_{total} = 1.00 \times 10^{-3}$ bar, $P_{O_2} = 2.12 \times 10^{-4}$ bar. Passive oxidation is denoted by the shaded region.

V.B.1. Oxidation-Nitridation Coupling

Rosner and Allendorf investigated individual oxidation and nitridation of SiC using molecular and atomic species of both elements. Molecular and atomic oxygen had similarly high oxidation rates with SiC, but the nitridation rate of SiC with molecular nitrogen was five orders of magnitude lower than that of atomic nitrogen.[18]

For atomic oxygen and nitrogen, Rosner and Allendorf also demonstrated that mass loss rates for *combined* oxidation and nitridation of SiC are an order of magnitude *less* than one would expect given independent oxidation and nitridation.[6] They attributed this effect to "coupling" between atomic nitrogen and oxygen. It is hypothesized that molecular nitrogen is relatively inert with SiC, but atomic nitrogen is not, since atomic nitrogen has a lower barrier for reactions than molecular nitrogen. Hald even proposed that atomic nitrogen acts as a catalyst for silicon reactions at the surface.[7]

It is inferred from the increased B'_{crit} for air versus O_2 in Fig. 9 (0.30 and 0.21, respectively) that air is more reactive with SiC due to the addition of nitrogen, which has minor effects on the oxidation behavior. However, at the temperatures for which SiC oxidizes actively, nitrogen is negligibly dissociated in standard air, and any coupling effects should be small. The significance of nitridation due to *atomic* nitrogen should increase at higher temperatures and relative concentrations than considered in this work, and warrants further investigation.

V.C. Mass Loss Rates under Active Oxidation

In the chemical equilibrium analysis, the *normalized* mass loss rate B' depends only on temperature and oxygen/total pressure. Note that B' is not strictly related to the oxidation kinetics, since it is not associated with a specific oxidation reaction, and includes contributions from sublimation and vaporization. Rather, B' is simply the mass flux from the surface required to maintain equilibrium of the gas-surface interface in the open system.

Mass loss rates in the active oxidation regime have been measured in several experiments, particularly those of Rosner and Allendorf,[6,18] and Narushima *et al.*[19] In the active regime, modeling results from Fig. 5 can be directly compared to the experimental data from Rosner and Allendorf.[18] The B' value is analogous to the "removal probability" ε defined by Rosner and Allendorf. ε is mole-based, while B' is mass-based. Thus, starting with Eq. (12), we can express ε in terms of B':

$$\varepsilon = \frac{J_{Si,C}}{J_{O_2}} = B' \frac{M_e}{M_w} \frac{X_{w,C}}{X_{e,O_2}} \tag{25}$$

$J_{Si,C}$ is the number flux of silicon or carbon atoms away from the surface (in any molecular configuration), M_e is the molecular weight of the edge gas mixture, and $X_{w,C}$ is the *elemental* mole fraction of carbon at the surface. For these dilute argon mixtures, the molecular weight ratio of the wall gas to the bulk gas is nearly unity. The results of this comparison are shown in Fig. 11, and very good agreement between measurement and analysis is obtained at temperatures above 2200 K.

Agreement at higher temperatures suggests the surface is likely in equilibrium, as the bulk oxidation rate agrees well with the equilibrium rate. Below ~1900 K (near the transition region), the observed oxidation

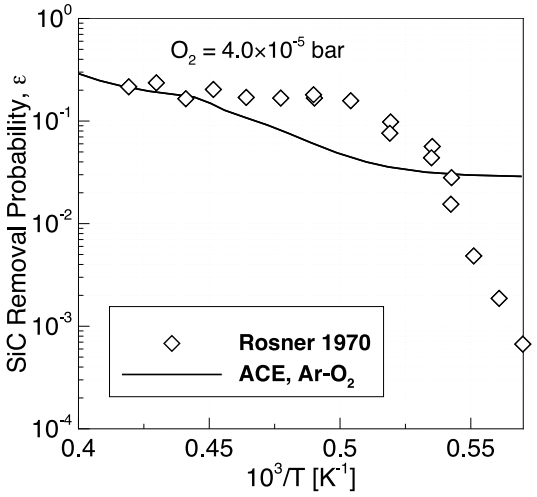

Figure 11: SiC removal probability for SiC-Ar/O_2, $P_{total} = 1.3 \times 10^{-3}$ bar, $P_{O_2} = 4.0 \times 10^{-5}$ bar.

rate is significantly lower than the equilibrium oxidation rate. This is indicative of kinetic barriers to reaching equilibrium, and reaction-limited effects.

VI. Model Application

VI.A. Application to Passive-to-Active Transition

Although multiple equilibrium states may exist at the *same* temperature and oxygen pressure, each exhibits different thermodynamic properties and mass loss rates. The path that the system will follow minimizes the free energy at the surface for each temperature, and other equilibrium solutions at that temperature are thermodynamically unstable. Once the system transitions from passive to active oxidation, A-P mechanisms such as attainment of sufficient SiO(g) pressure at the surface prevent transition back to a passive state.

There are two mechanisms for P-A transition: constant pressure thermal oxidation, and decreasing oxygen pressure at constant temperature (TGA-type). The mechanism for thermal oxidation of SiC at constant pressure is described in Fig. 12. Relative to Figs. 5 and 9, the axes are inverted to demonstrate temperature dependence. Gibbs free energy of the mixture determines thermodynamic stability and behavior, and the B' parameter describes the relative flux of oxidation products from the surface. The proposed thermal oxidation mechanism for SiC is presented in Fig. 12 with the solid line. At 5.0×10^{-2} bar air, passive oxidation occurs below 1800K. As surface temperature increases further, the mechanism is described in detail as follows:

1. In the passive oxidation state between $\boxed{1} \rightarrow \boxed{2}$, only one equilibrium solution exists, and the B' values indicate that the SiO_2(s) surface is relatively inert.

2. Around 2000 K, multiple equilibrium solutions exist at states $\boxed{2}$ and $\boxed{4}$. State $\boxed{2}$ is in the passive

oxidation regime, but 4 is the transition to active oxidation. However, the free energy at state 4 is actually lower than state 2, and suggests that 4 is thermodynamically favored. Thus, it follows that P-A transition occurs directly from 2 → 4, and is discontinuous with respect to mixture thermodynamic properties and mass loss rates.

3. Above 2000 K, the predicted path is 4 → 5, and the surface is actively oxidizing. Other states are thermodynamically unstable, shown in Fig. 12 with dashed lines. Although path 4 → 3 has a lower free energy overall, this would imply transition back to the passive state, which is physically unattainable due to A-P mechanisms.

4. Above 2500 K for states 5 → 6, the surface is still oxidizing actively, and there is again only one equilibrium solution. The B' plot indicates that the surface mass loss rate increases rapidly beyond 2500 K.

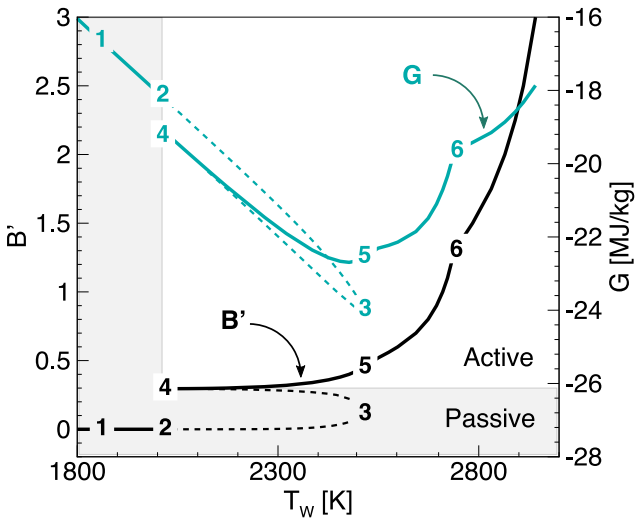

Figure 12: Modified B' plot for passive-to-active transition via thermal oxidation at constant pressure at 5.0×10^{-2} bar air. Dashed lines denote solutions that are thermodynamically unstable, and passive states are in the shaded region.

VI.B. Temperature Jump: 1-D Material Response Analysis

The temperature jump is observed when SiC composites are heated and undergo P-A transition via thermal oxidation in dissociated/recombining plasma flows.[8,9] It is not clear if this phenomenon occurs for pure SiC as well, and not just for SiC composites, since pure SiC has not been studied in such facilities to the authors' knowledge. Previous studies have proposed that the jump is due to an increase in surface recombination/catalycity during P-A transition from exposed SiC.[7–9]

The thermal oxidation mechanism in Fig. 12 is applied to material response test cases to evaluate the effect of P-A transition on surface temperature. Material response analyses involve transient in-depth

heat conduction calculations, and mixture thermodynamic properties and mass loss rates directly affect the surface energy balance. Using the thermodynamic model for material-environment interactions, these results are valid when chemical kinetic rates are much faster than the conduction timescales.

Table 1: Aerothermal Heating Parameters (Air)

Test Case	P_{air} [bar]	h_e $[\frac{MJ}{kg}]$	$\rho_e u_e C_H$ $[\frac{kg}{m^2-s}]$
MTA-12	5.0×10^{-2}	5.3*	0.264
HER-17	2.0×10^{-2}	6.0*	0.216

* Bulk enthalpy estimated with electrical coupling efficiency $\eta = 0.3$, and $h_e = \eta P_{el}/\dot{m}$

Table 1 summarizes two conditions taken from Panerai *et al.*,[9] where temperature jump was demonstrated to occur for a C-SiC composite. For the MTA-12 case, static air pressure is 5.0×10^{-2} bar, and flow enthalpy is approximated as 5.3 MJ/kg using the electric input power of 283 kW, mass flowrate of 16 g/s, and assuming a coupling efficiency of 0.3. Using the measured cold-wall heat flux of 1403 kW/m^2, this results in an aerothermal heating coefficient of $\rho_e u_e C_H = 0.264$ kg/m^2-s, according to Eq. (8).

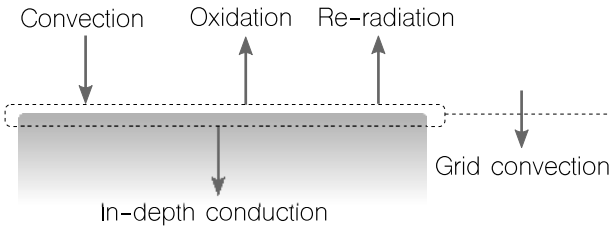

Figure 13: Surface energy balance for material response boundary condition. Grid convection is due to the moving boundary when surface recession occurs.

The transient one-dimensional heat conduction equation, Eq. (26), is solved numerically over a 0.1 m domain, with an initial temperature of 400 K. Material thermal conductivity, heat capacity, and density are representative of homogeneous SiC, and are temperature-dependent.

$$\frac{\partial T}{\partial t} = \frac{\kappa}{\rho_s C_p}\frac{\partial^2 T}{\partial x^2} \tag{26}$$

$$\overbrace{-\kappa\frac{\partial T}{\partial x}}^{\text{conduction}} = \overbrace{\rho_e u_e C_H (h_e - h_w)}^{\text{convection}} - \overbrace{\epsilon\sigma(T_w^4 - T_\infty^4)}^{\text{re-radiation}} - \overbrace{\rho_s \dot{s} h_w}^{\text{oxidation}} + \overbrace{\rho_w \dot{s} h_w}^{\text{grid convection}} \tag{27}$$

$$\dot{s} = B' \frac{\rho_e u_e C_M}{\rho_s} \tag{28}$$

The surface energy balance is illustrated in Fig. 13, and each component is described in Eq. (27). Surface recession rate $\dot{s}$ is determined from Eq. (28). At each timestep, the conduction term from Eq. (27) is computed and imposed on the boundary of the domain, opposite an adiabatic wall. Unity Lewis number is assumed, and re-radiation from the surface is estimated with emissivity $\epsilon = 0.8$ and farfield temperature

$T_\infty = 300$ K. The results from Fig. 12 are tabulated, and provide B' and h_w values as a function of surface temperature. Closure of the SEB equation is then obtained by iterating upon the B', T_w, and h_w values.

Table 2: Material Response Results

Test Case	T_w	Experiment	Simulation	% Error
MTA-12	Pre-jump	2064 K	2012 K	2.52%
MTA-12	Post-jump	2542 K	2540 K	0.08%
HER-17	Pre-jump	2115 K	1952 K	7.71%
HER-17	Post-jump	2512 K	2420 K	3.66%

The predicted surface temperature over time is shown in Fig. 14, and exhibits a temperature jump around 200 s that corresponds to the bifurcation between passive and active states in Fig. 12. The time that the temperature jump occurs is not important for this comparison, but both pre- and post-jump temperatures in Table 2 are within 8% of those observed in the experiment. These results demonstrate a clear relationship between temperature jump and the thermal oxidation mechanism of SiC, and predicts the temperature jump behavior with a thermodynamic equilibrium approach. However, more detailed conclusions should not be made since flowfield conditions are only approximated, and the effect of differences in geometry and material needs to be evaluated.

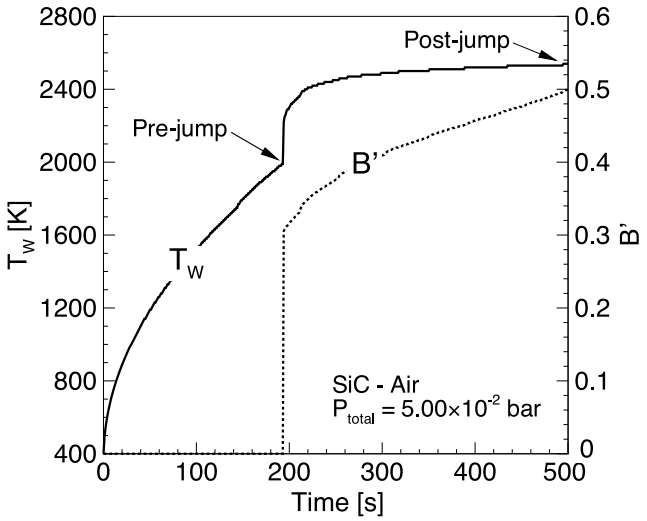

Figure 14: Surface temperature vs. time for the MTA-12 test case (5.0×10^{-2} bar air). Note temperature jump occurs at 200 s, corresponding to a sharp increase in surface mass loss (B'). The pre-jump temperature corresponds to the passive-to-active transition point.

VII. Summary and Conclusions

The thermodynamics of silicon carbide oxidation were examined with a chemical equilibrium approach. In contrast to previous works, an open-system mass balance with a boundary layer diffusion approximation

provided more accurate and relevant calculations for the thermodynamics of passive-to-active oxidation in silicon carbide. Additionally, concentrations of species in the gaseous phase were computed for both ambient oxygen and air environments, and predominant condensed species in equilibrium with the gaseous phase were determined. This model described the mixture thermodynamic properties and surface mass loss in passive and active states, which explained the temperature jump phenomenon observed in thermal oxidation experiments.

The silicon carbide oxidation model was evaluated for several metrics against available experimental data in the literature. Notably, passive-to-active transition conditions in oxygen and air agreed with experimental transition data obtained in the diffusion-limited regime within an order of magnitude oxygen pressure. Although a distinction was made between oxygen and air environments, the model suggests that this is perhaps unnecessary when predicting the transition temperature, as differences of only 3% are observed. When the model was applied to material response calculations for thermal oxidation of silicon carbide, pre- and post-jump surface temperatures agreed with experimental measurements for SiC within 8%.

This work demonstrates the importance of using an open (rather than a closed) system when performing chemical equilibrium calculations, which necessitates consideration of mass transport in the boundary layer. Furthermore, this work improves understanding of the thermodynamics during SiC oxidation. The passive-to-active thermal oxidation mechanism and the temperature jump effect were described under constant pressure conditions. However, in hypersonic flight applications, oxidation transitions occur in environments with varying temperature and pressure. These transition mechanisms need to be explored to better understand discrepancies between theoretical and experimental measurements.

Acknowledgments

The authors acknowledge support through funding from the U.S. Office of Naval Research, Grant N00014-18-1-2531.

References

[1]Parthasarathy TA, Rapp RA, Opeka M, Kerans RJ. A model for the oxidation of ZrB_2, HfB_2 and TiB_2. Act. Mat. 2007;55(17):5999-6010.

[2]Hinze JW, Graham HC. The Active Oxidation of Si and SiC in the Viscous Gas-Flow Regime. J. Elec. Soc. 1976;123(7):1066-1073.

[3]Jacobson N, Harder B, Myers D. Oxidation transitions for SiC part I. Active-to-passive transitions. J. Am. Cer. Soc. 2013;96(3):838-844.

[4]Balat M. Determination of the Active-to-Passive Transition in the Oxidation of Silicon Carbide in Standard and Microwave-Excited Air. J. Eur. Cer. Soc. 1996;16(1):55-62.

[5]Harder B, Jacobson N, Myers D. Oxidation transitions for SiC part II. Passive-to-active transitions. J. Am. Cer. Soc. 2013;96(2):606-612.

[6]Rosner DE, Allendorf, HD. Nitrogen as an Ablative Reactant in Dissociated Air. AIAA J. 1970;8(1):166-168.

[7]Hald H. Operational limits for reusable space transportation systems due to physical boundaries of C/SiC materials. Aero. Sci. Tech. 2003;7(7):551-559.

[8]Marschall J, Pejakovic D, Fahrenholtz WG, Hilmas GE, Panerai F, Chazot O. Temperature jump phenomenon during plasmatron testing of ZrB_2-SiC ultrahigh-temperature ceramics. J. Ther. Heat Tran. 2012;26(3):559-572.

[9]Panerai F, Helber B, Chazot O, Balat-Pichelin M. Surface temperature jump beyond active oxidation of carbon/silicon carbide composites in extreme aerothermal conditions. Carbon. 2014;7:102-119.

[10]Wang J, Zhang L, Zeng Q, Vignoles GL, Guette A. Theoretical investigation for the active-to-passive transition in the oxidation of silicon carbide. J. Am. Cer. Soc. 2008;91(5):1665-1673.

[11]Poerschke DL, Novak MD, Abdul-Jabbar N, Krämer S, Levi CG. Selective active oxidation in hafnium boride-silicon carbide composites above 2000 °C. J. Eur. Cer. Soc. 2016;36(15):3697-3707.

[12]Dawi K, Balat-Pichelin M, Charpentier L, Audubert F. High temperature oxidation of SiC under helium with low-pressure oxygen. Part 3: β-SiC-SiC/PyC/SiC. J. Eur. Cer. Soc. 2012;32(2):485-494.

[13]Charpentier L, Balat-Pichelin M, Glenat H, Beche E, Laborde E, Audubert F. High temperature oxidation of SiC under helium with low-pressure oxygen. Part 2: CVD β-SiC. J. Eur. Cer. Soc. 2010;30(12):2661-2670.

[14]Charpentier L, Balat-Pichelin M, Audubert F. High temperature oxidation of SiC under helium with low-pressure oxygen. Part 1: Sintered α-SiC. J. Eur. Cer. Soc. 2010;30(12):2653-2660.

[15]Ogura Y, Morimoto T. Mass Spectrometric Study of Oxidation of SiC in Low-Pressure Oxygen. J. Elec. Soc. 2002;149(4):47-52.

[16]Gulbransen EA, Andrew KF, Brassart FA. The Oxidation of Silicon Carbide at 1150° C to 1400° C and at 9×10^{-3} to 5×10^{-1} Torr Oxygen Pressure. J. Elec. Soc. 1966;113(12):1311-1314.

[17]Keys LH. The Oxidation of Silicon Carbide. In: Foroulis ZA, Pettit FS, editors. Properties of High Temperature Alloys With an Emphasis on Environmental Effect. Princeton: Electrochemical Society, 1977; p. 681-697.

[18]Rosner DE, Allendorf HD. High temperature kinetics of the oxidation and nitridation of pyrolytic silicon carbide in dissociated gases. J. Phys. Chem. 1970;74(9):1829-1839.

[19]Narushima T, Iguchi Y, Hirai T. High-Temperature Active Oxidation of Chemically Vapor-Deposited Silicon Carbide in an Ar-O_2 Atmosphere. J. Am. Cer. Soc. 1991;74(10):2583-2586.

[20]Jacobson N, Myers D. Active oxidation of SiC. Oxid. Met. 2011;75:1-25.

[21]Chase Jr MW. NIST-JANAF Thermochemical Tables. 4th ed. New York: American Institute of Physics; 1998.

[22]Bard AJ. Calculation of Equilibrium Constants from Free Energy Data. In: Rice SA, editor. Chemical Equilibrium. New York: Harper & Row, 1966; p. 182-185.

[23]Wagner C. Passivity during the oxidation of silicon at elevated temperatures. J. Appl. Phys. 1958;29(9):1295-1297.

[24]Turkdogan ET, Grieveson P, Darken LS. Enhancement of diffusion-limited rates of vaporization of metals. J. Phys. Chem. 1963;67(8):1647-1654.

[25]Heuer AH, Lou VLK. Volatility Diagrams for Silica, Silicon Nitride, and Silicon Carbide and Their Application to High Temperature Decomposition and Oxidation. J. Am. Cer. Soc. 1990;73(10):2789-2803.

[26]Sakraker I, Asma CO. Experimental investigation of passive/active oxidation behavior of SiC based ceramic thermal protection materials exposed to high enthalpy plasma. J. Eur. Cer. Soc. 2013;33(2):351-359.

[27]Song Y, Dhar S, Feldman LC, Chung G, Williams JR. Modified Deal Grove model for the thermal oxidation of silicon carbide. J. Appl. Phys. 2004;95(9):4953-4957.

[28]Bartlett EP, Kendall RM, Rindal RA. An Analysis of the Coupled Chemically Reacting Boundary Layer and Charring Ablator. Part IV: A Unified Approximation for Mixture Transport Properties for Multicomponent Boundary Layer Applications. NASA; 1968. Itek Corporation, Vidya Division. NASA CR-1063.

[29]Powars CA, Kendall RM. Aerotherm Chemical Equilibrium (ACE) Computer Program - Users Manual. Mountain View: Aerotherm Corporation; 1969.

[30]Muehlhoff L, Choyke WJ, Bozack MJ, Yates JT. Comparative electron spectroscopic studies of surface segregation on SiC(0001) and SiC(000$\bar{1}$). J. Appl. Phys. 1986;60(8):2842-2853.

[31]Fegley Jr MB. The Thermodynamic Properties of Silicon Oxynitride. J. Am. Cer. Soc. 1981;64(9):124126.

[32]Vaughn WL, Maahs HG. Active-to-Passive Transition in the Oxidation of Silicon Carbide and Silicon Nitride in Air. J. Am. Cer. Soc. 1990;73(6):1540-1543.

Figure Caption List

Figure 1: Summary of experimental (symbols) and theoretical (lines) transition conditions for SiC-O_2. Data for air is excluded. Both active-to-passive and passive-to-active transitions are shown, and correspond to active-to-passive unless otherwise indicated.

Figure 2: Wagner model for active SiC oxidation.

Figure 3: Wagner model applied to passive SiO_2 vaporization.

Figure 4: Open system mass balance in ACE. Three regions are present: the boundary layer edge, the gas-surface interface, and the bulk material. O_2 species represent the flux $\rho_e u_e C_M$ from the ambient to the surface, and SiO/CO represent the flux of oxidation products away from the surface $\dot{m}_w$. Flow outside the boundary layer is $\rho_e u_e$.

Figure 5: B' plot for the SiC-Ar/O_2 system, $P_{total} = 1.00 \times 10^{-3}$ bar, $P_{O_2} = 2.12 \times 10^{-4}$ bar. The transition point separates passive (SiO_2) and active (SiC) regimes.

Figure 6: Gas-phase equilibrium species composition for the SiC-Ar/O_2 system, $P_{total} = 1.00 \times 10^{-3}$ bar, $P_{O_2} = 2.12 \times 10^{-4}$ bar. Passive oxidation is denoted by the shaded region.

Figure 7: Predominant surface phase maps for the SiC-Ar/O_2 system at constant total pressure of 1.0 bar, (a) as a function of B', and (b) as a function temperature. Passive-to-active oxidation transitions occur at the boundary of the SiO_2(s) stability region.

Figure 8: Oxidation transitions for the SiC-air system, both passive-to-active and active-to-passive. The Ar/O_2 transition is also shown for comparison. Symbols denote experimental data.

Figure 9: B' plot for SiC-air system, $P_{total} = 1.00 \times 10^{-3}$ bar, $P_{O_2} = 2.12 \times 10^{-4}$ bar. The SiC-Ar/O_2 case at equivalent P_{O_2} from Fig. 5 is shown for comparison. Shaded region corresponds to passive oxidation.

Figure 10: Gas-phase equilibrium species composition for the SiC-air system, $P_{total} = 1.00 \times 10^{-3}$ bar, $P_{O_2} = 2.12 \times 10^{-4}$ bar. Passive oxidation is denoted by the shaded region.

Figure 11: SiC removal probability for SiC-Ar/O_2, $P_{total} = 1.3 \times 10^{-3}$ bar, $P_{O_2} = 4.0 \times 10^{-5}$ bar.

Figure 12: Modified B' plot for passive-to-active transition via thermal oxidation at constant pressure at 5.0×10^{-2} bar air. Dashed lines denote solutions that are thermodynamically unstable, and passive states are in the shaded region.

Figure 13: Surface energy balance for material response boundary condition. Grid convection is due to the moving boundary when surface recession occurs.

Figure 14: Surface temperature vs. time for the MTA-12 test case (5.0×10^{-2} bar air). Note temperature jump occurs at 200 s, corresponding to a sharp increase in surface mass loss (B'). The pre-jump temperature corresponds to the passive-to-active transition point.

Table Caption List

Table 1: Aerothermal Heating Parameters (Air)

Table 2: Material Response Results

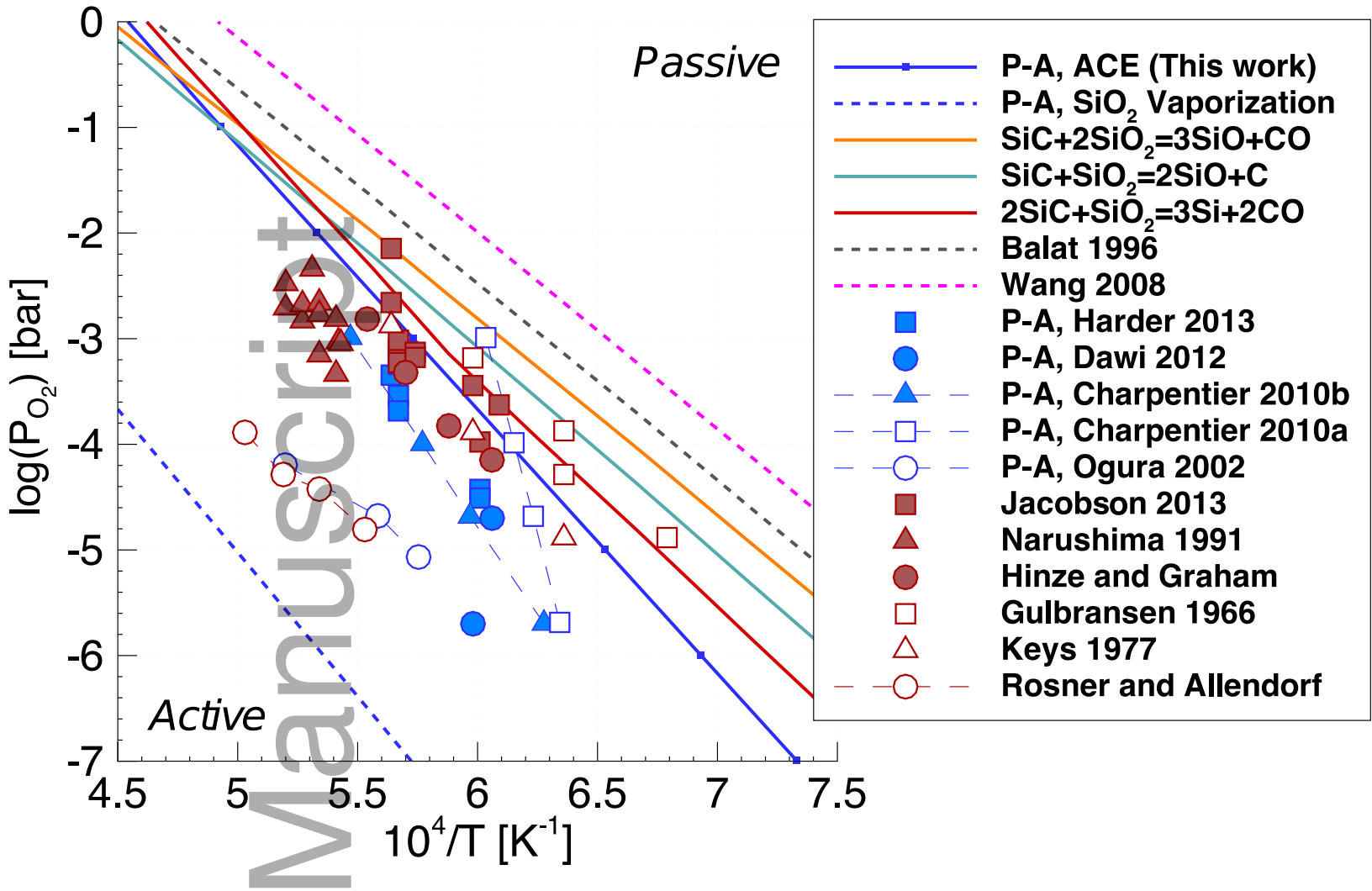

jace_16272_f1.eps

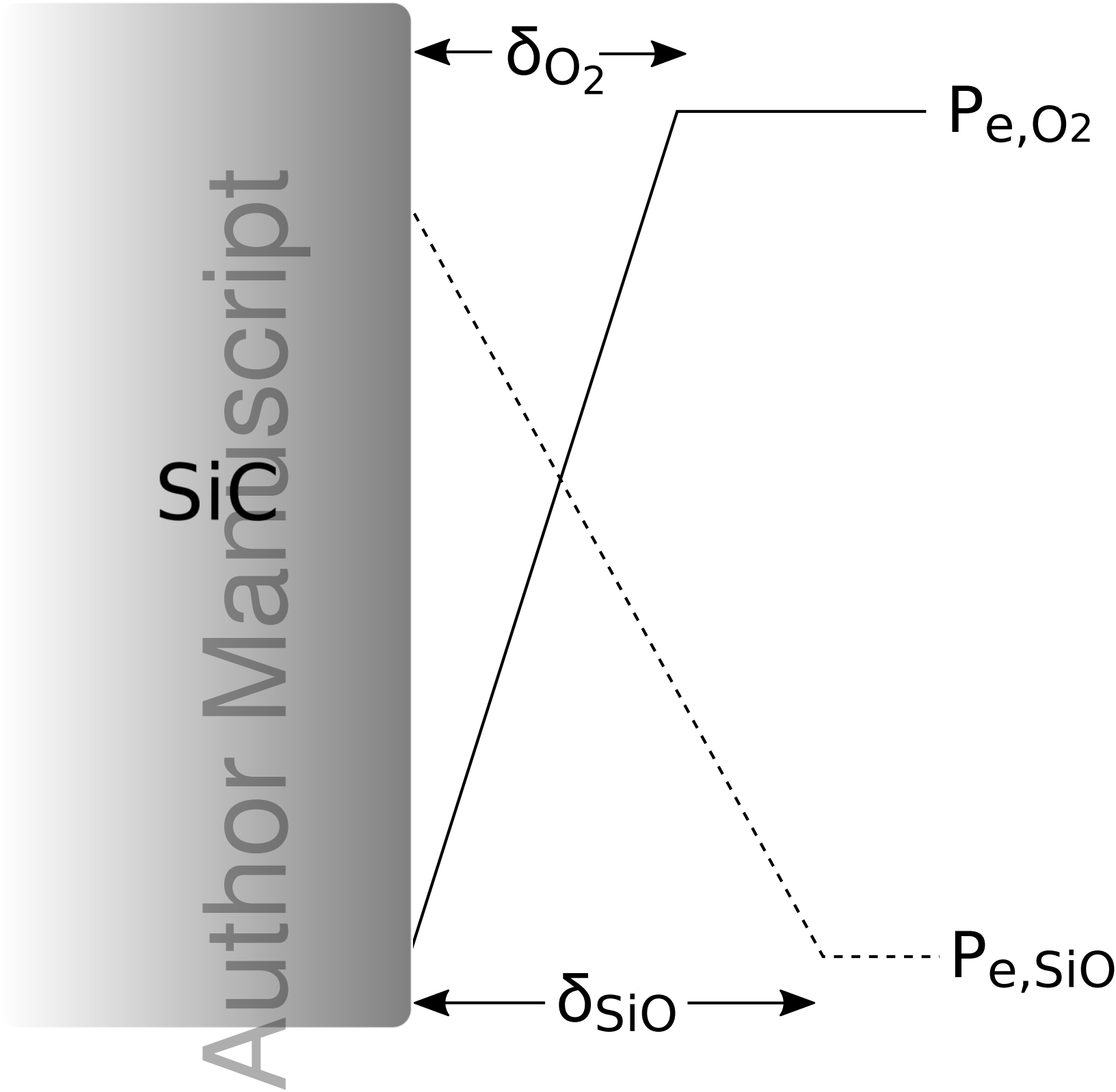

jace_16272_f2.eps

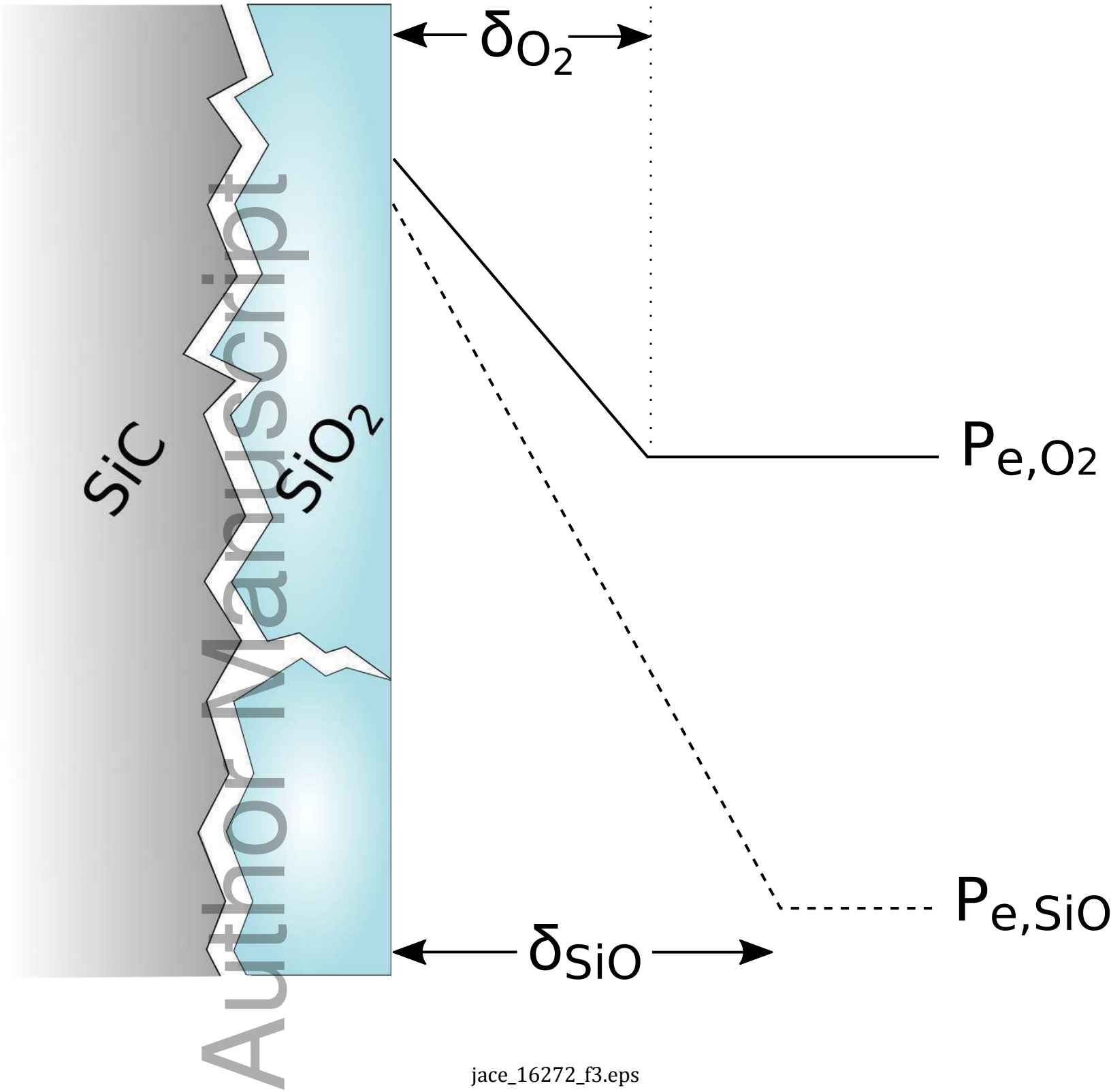

jace_16272_f3.eps

jace_16272_f4.eps

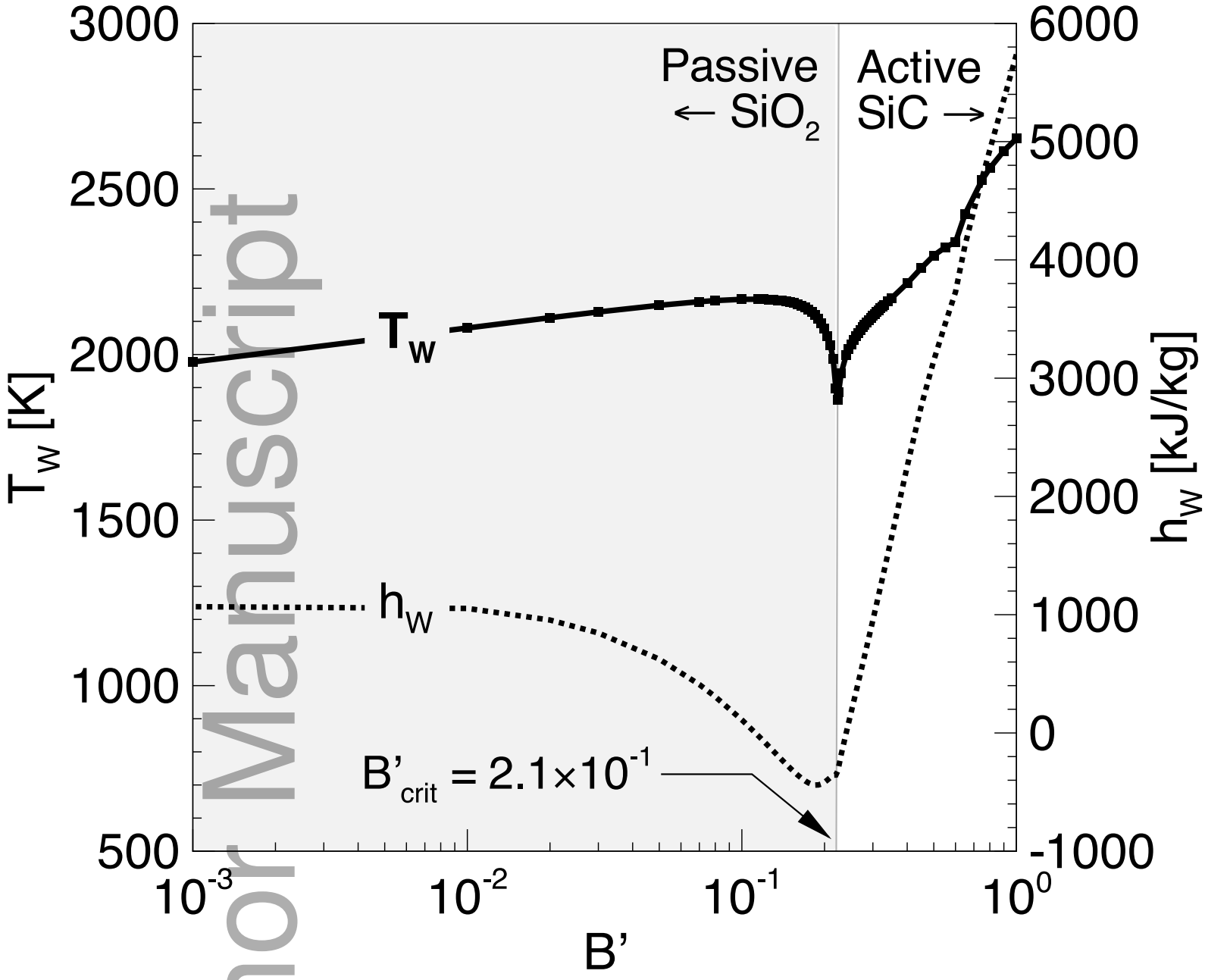

jace_16272_f5.eps

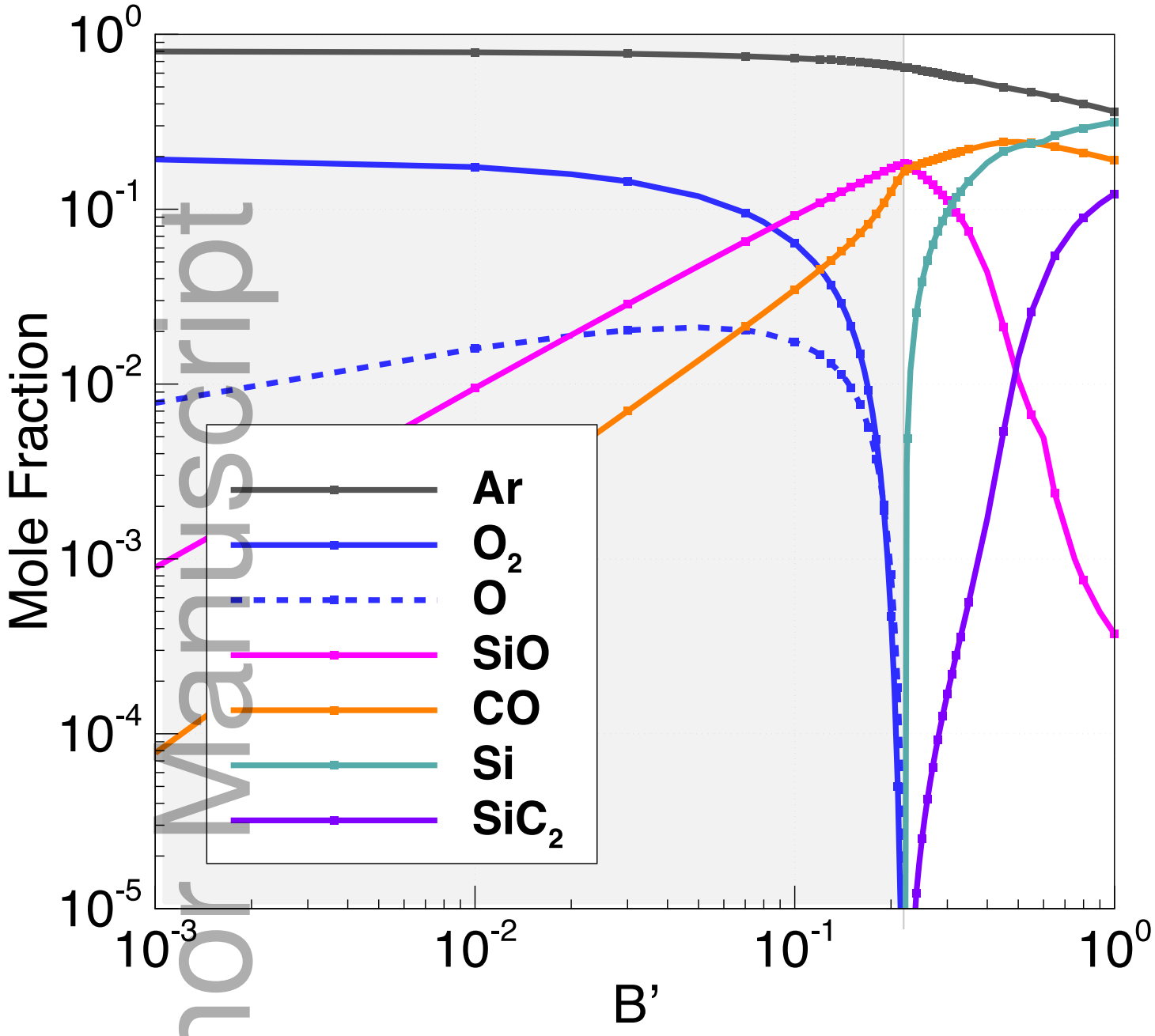

jace_16272_f6.eps

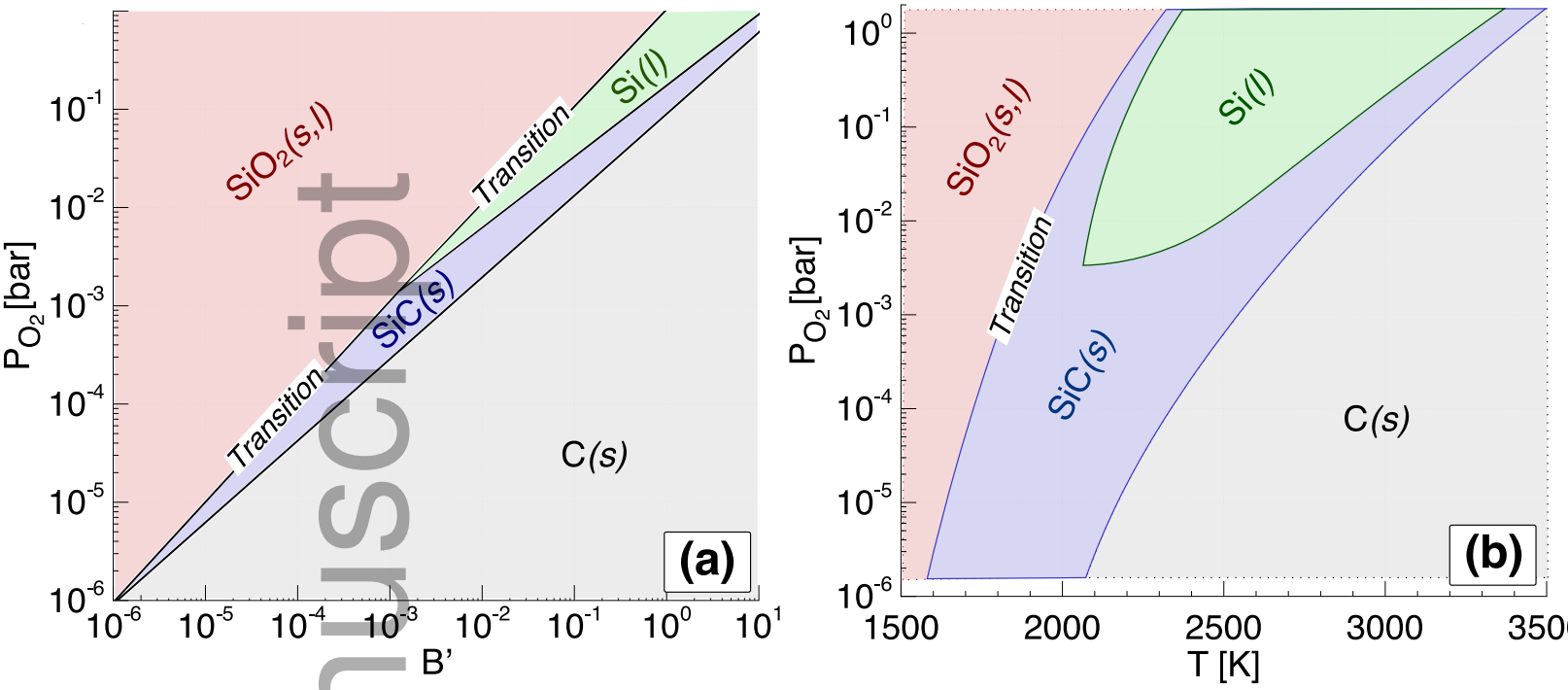

jace_16272_f7.eps

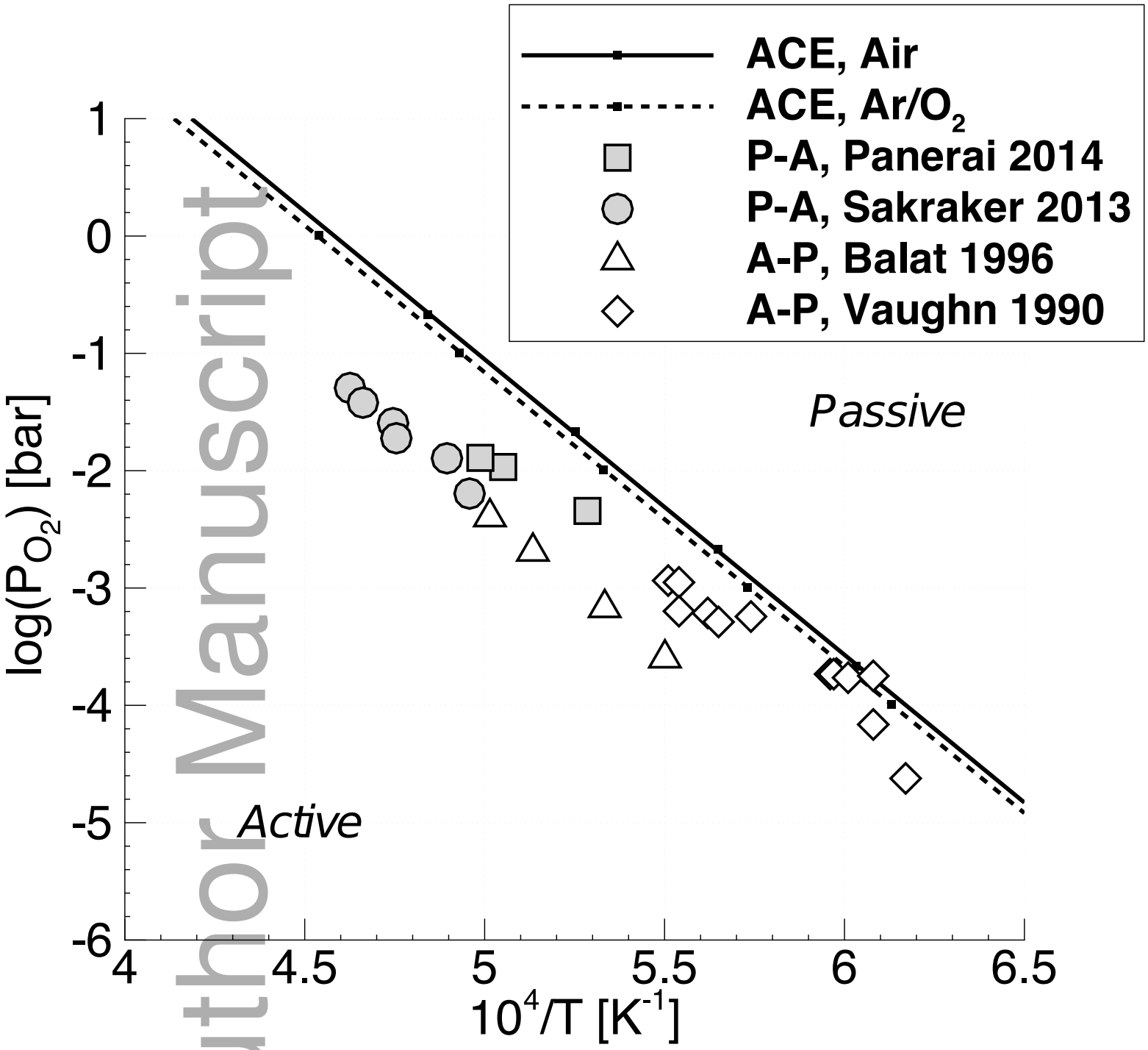

jace_16272_f8.eps

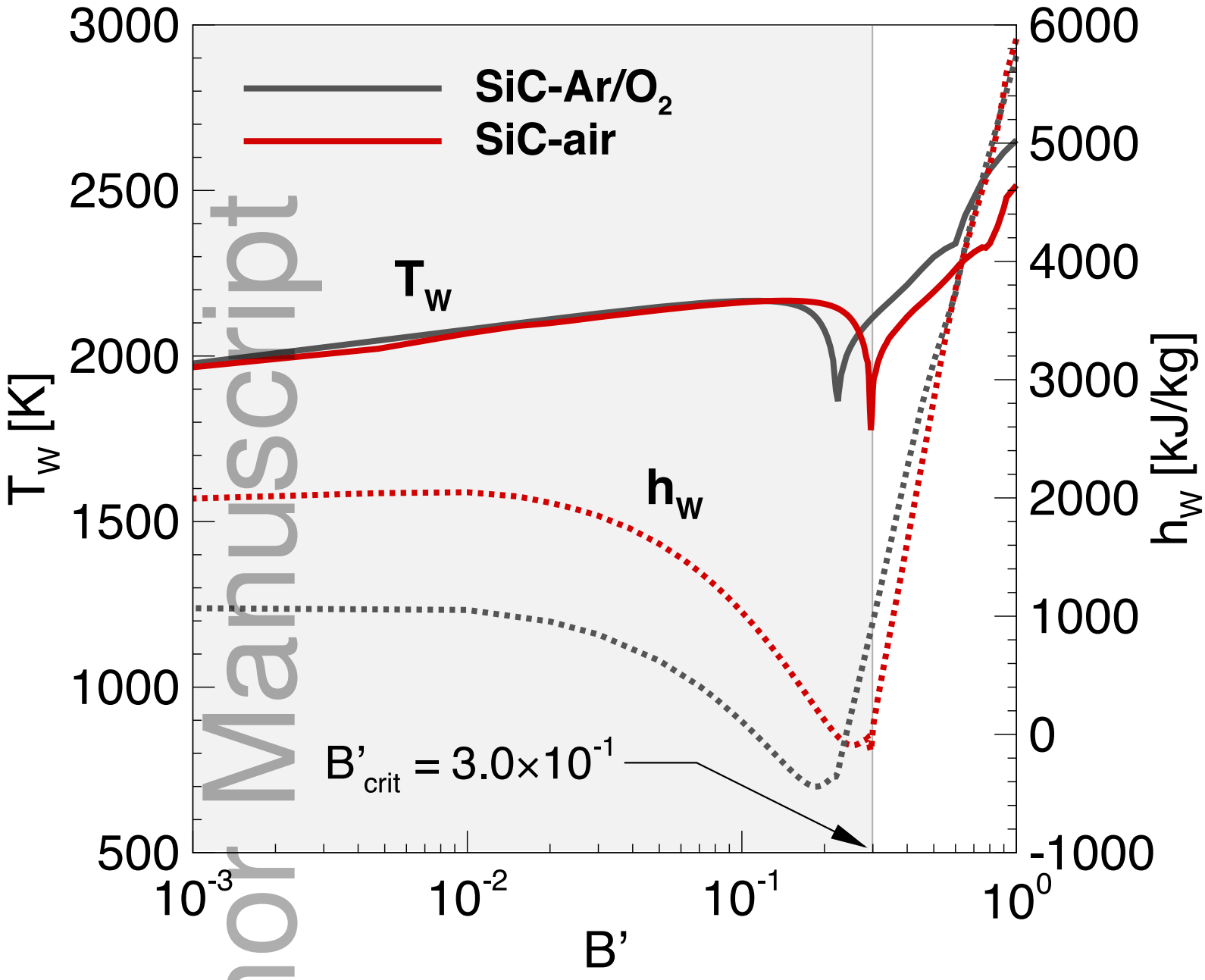

jace_16272_f9.eps

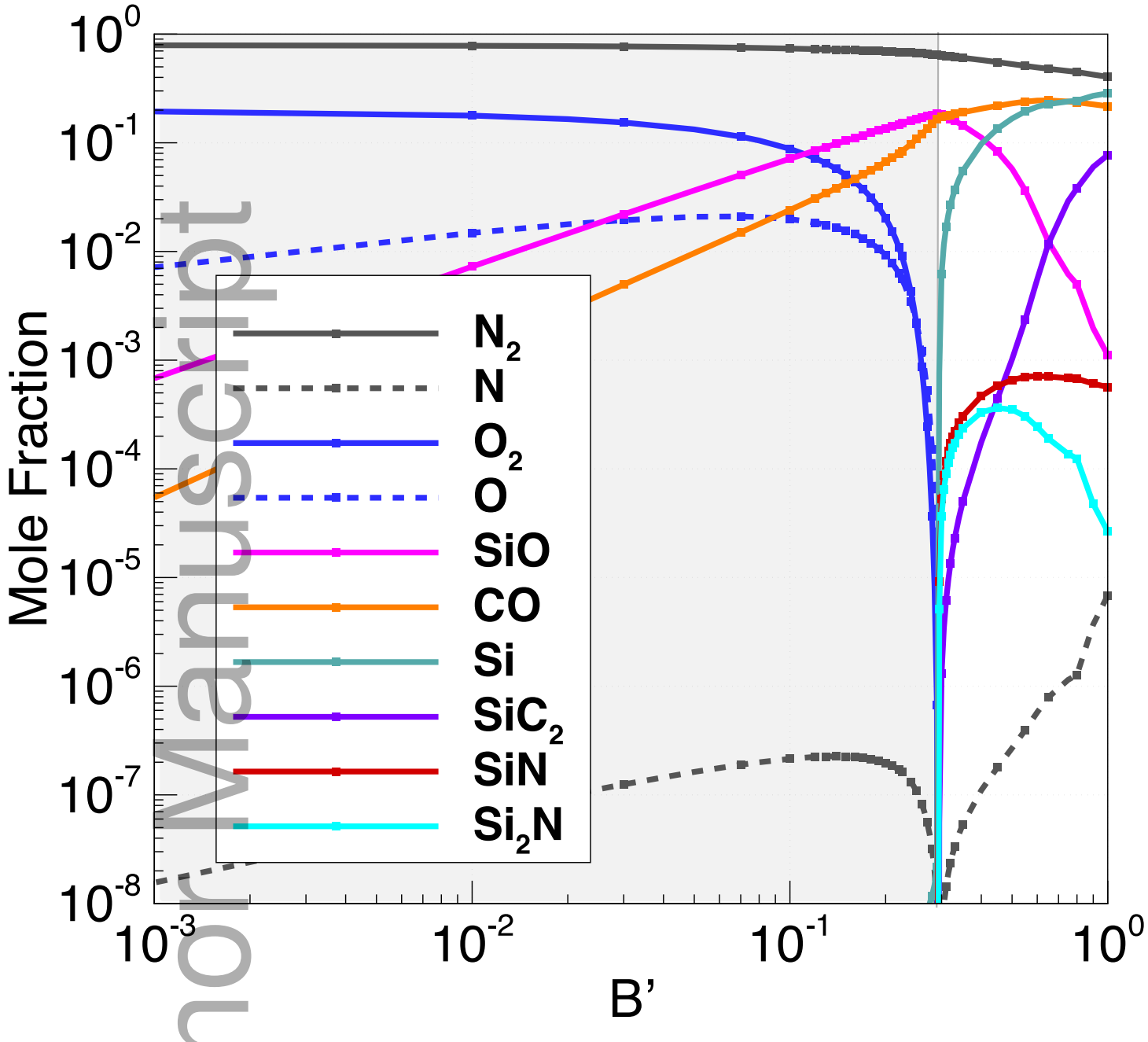

jace_16272_f10.eps

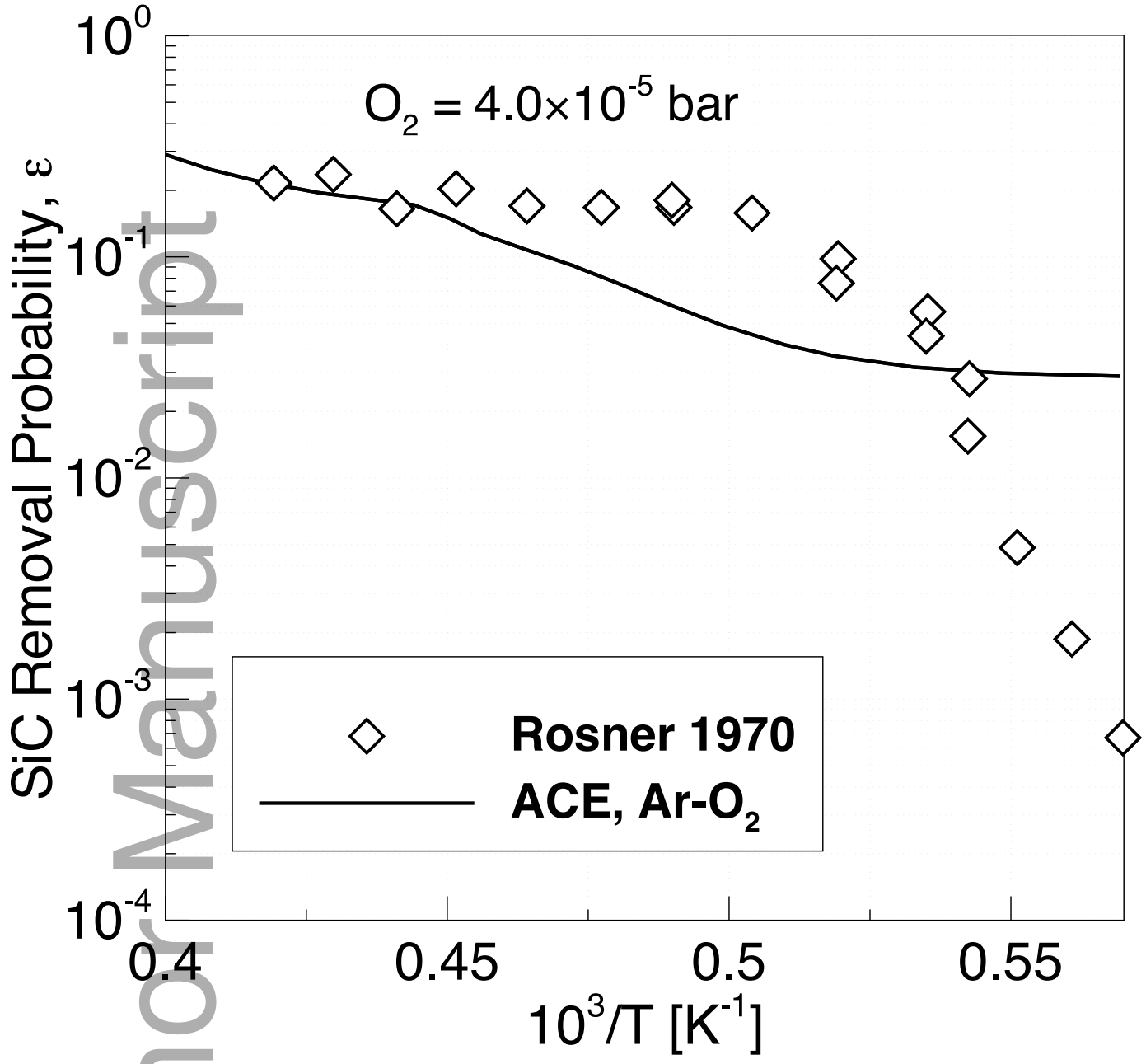

jace_16272_f11.eps

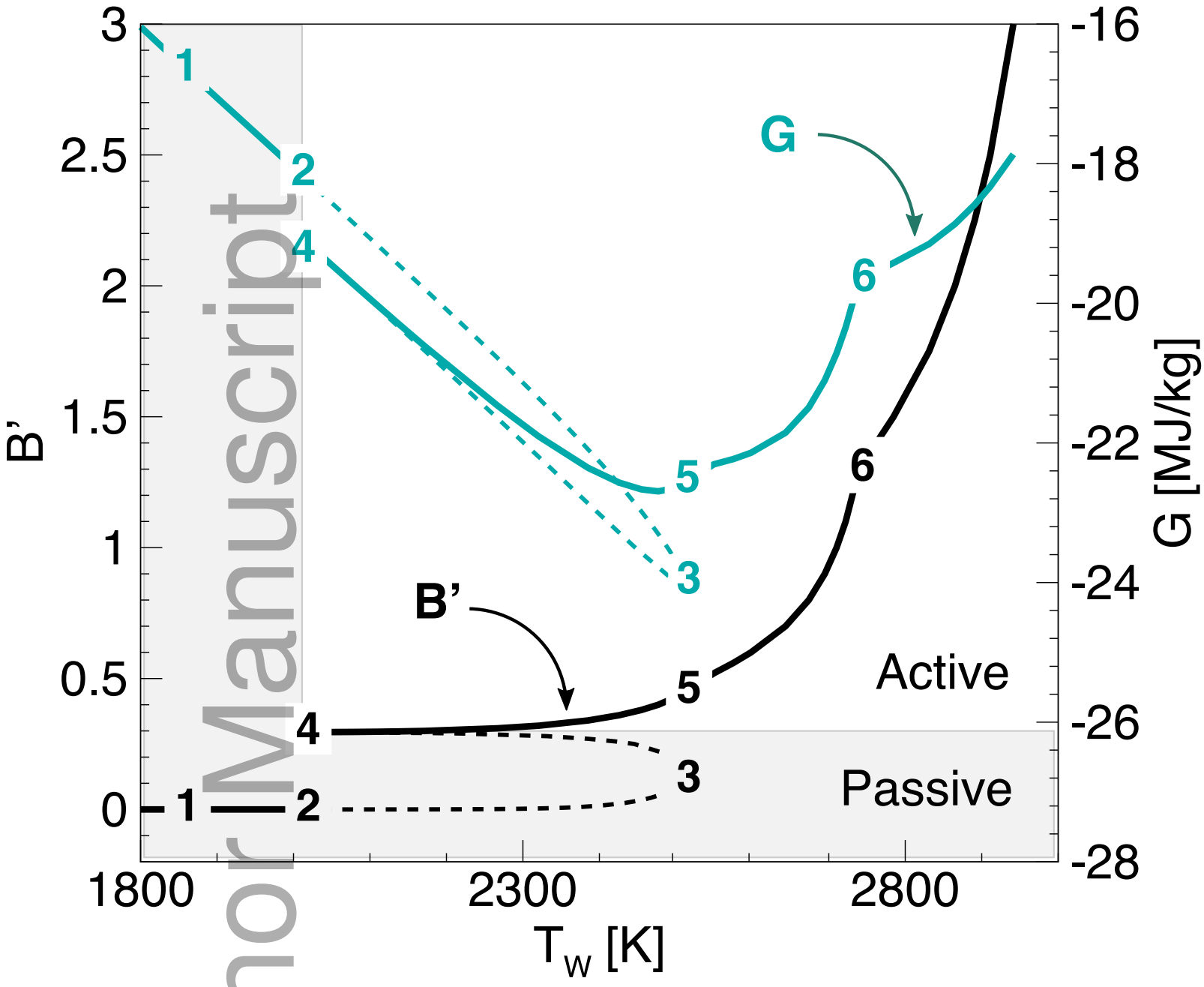

jace_16272_f12.eps

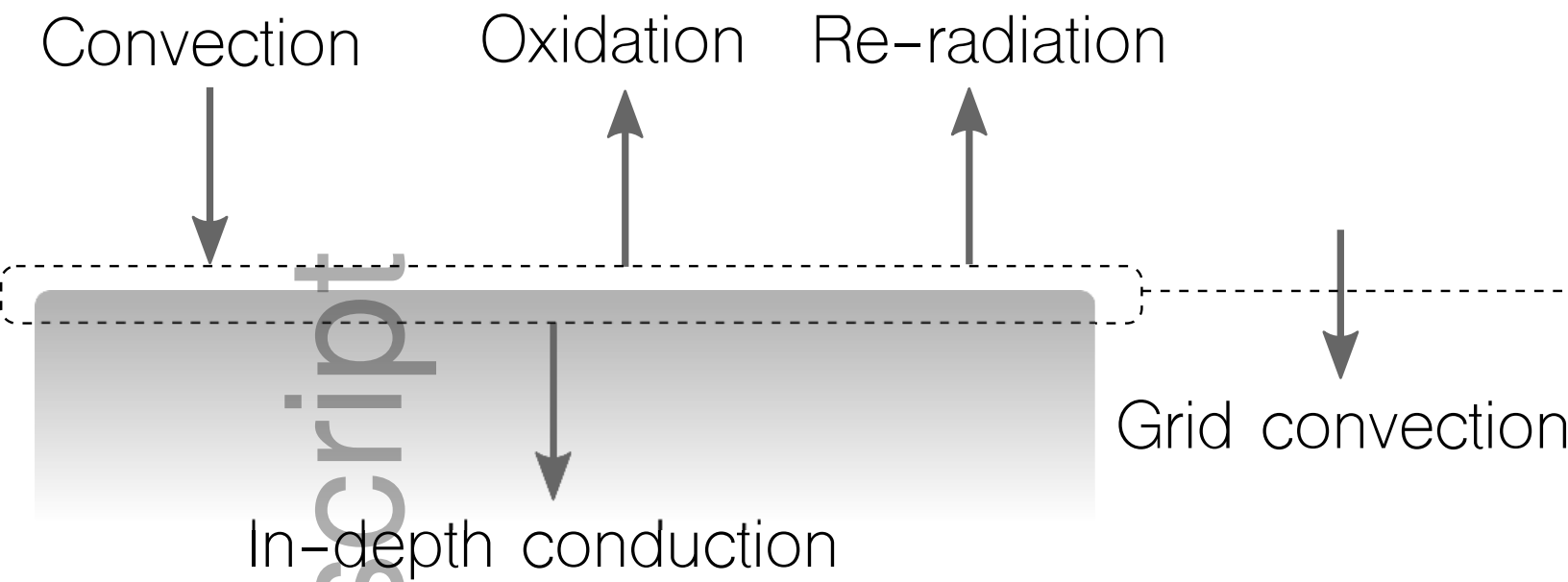

jace_16272_f13.eps

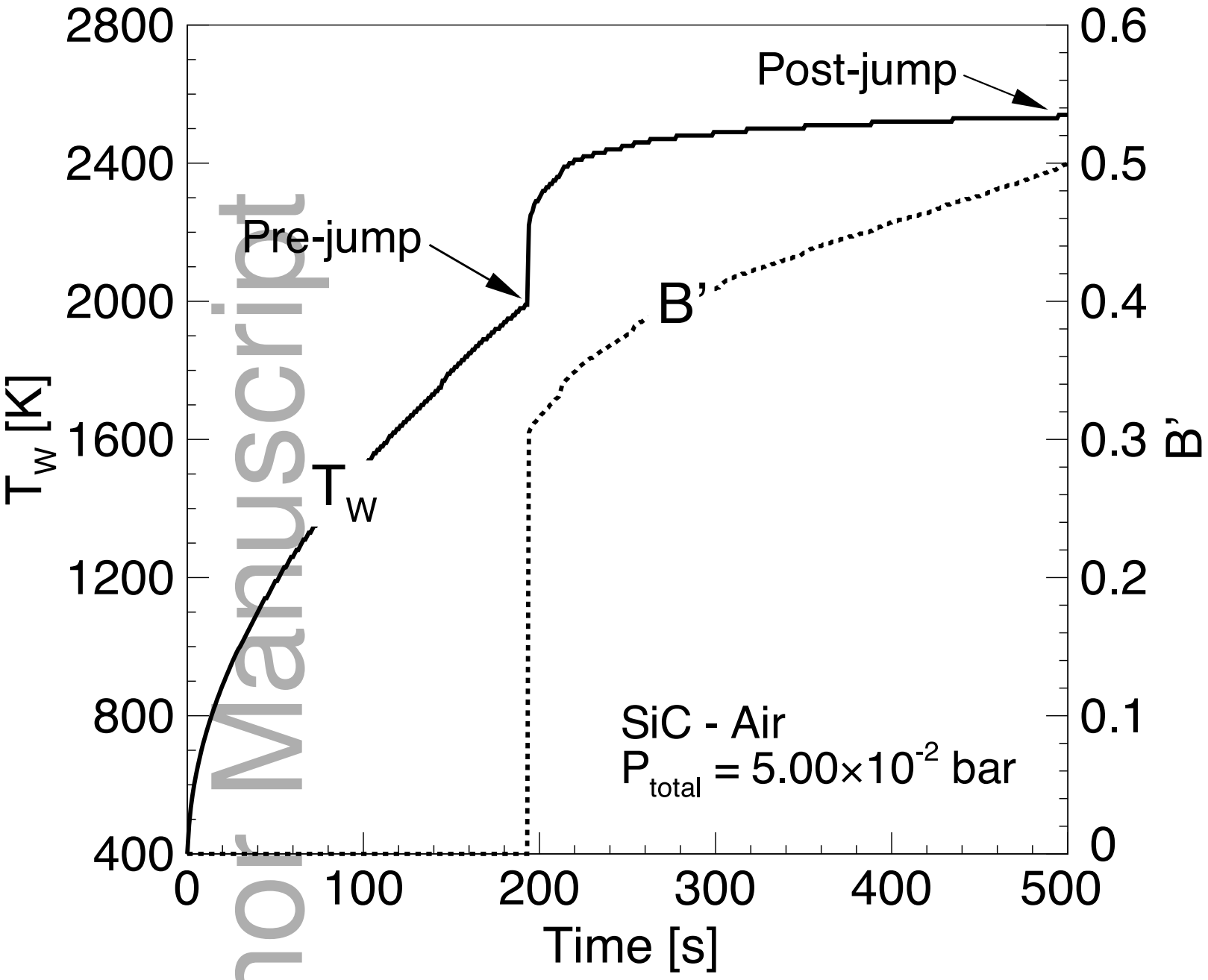

jace_16272_f14.eps